AD-A150 619 BEHAVIOUR OF FIBRE-REINFORCED COMPOSITES UNDER DYNAMIC TENSION(U) OXFORD UNIV (ENGLAND) DEPT OF ENGINEERING SCIENCE K SAKA ET AL. 21 AUG 84 AFOSR-TR-85-0063 1/1

UNCLASSIFIED AFOSR-82-0346 F/G 11/4 NL

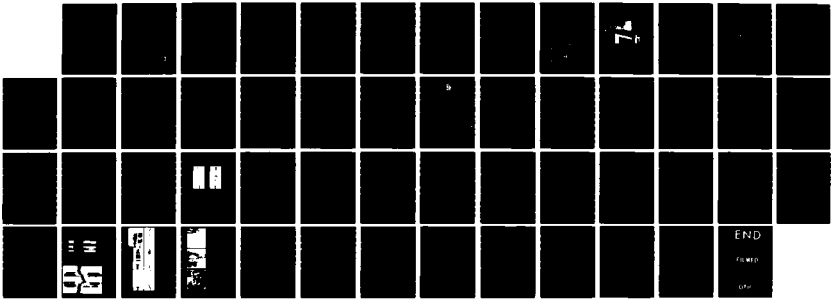

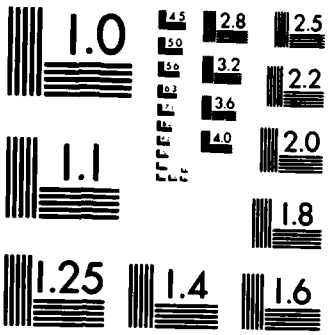

Grant No: AFOSR-82-0346

BEHAVIOUR OF FIBRE-REINFORCED COMPOSITES UNDER DYNAMIC TENSION

K Saka and J Harding
Department of Engineering Science
University of Oxford
Parks Road
OXFORD OX1 3PJ
UNITED KINGDOM

21st August, 1984

Final Report, 30th September 1982 - 14th March, 1984

Approved for public release; distribution unlimited

Prepared for:

AFOSR/NA
Building 410
Bolling AFB
D.C. 20332

and

European Office of Aerospace
Research & Development
London
ENGLAND

UNCLASSIFIED

SECURITY CLASSIFICATION OF THIS PAGE

REPORT DOCUMENTATION PAGE

1a. REPORT SECURITY CLASSIFICATION: Unclassified	1b. RESTRICTIVE MARKINGS
2a. SECURITY CLASSIFICATION AUTHORITY	3. DISTRIBUTION/AVAILABILITY OF REPORT: Approved for public release: distribution unlimited.
2b. DECLASSIFICATION/DOWNGRADING SCHEDULE	
4. PERFORMING ORGANIZATION REPORT NUMBER(S)	5. MONITORING ORGANIZATION REPORT NUMBER(S): AFOSR-TR- 85-0068
6a. NAME OF PERFORMING ORGANIZATION: Department of Engineering Science - UNIV OF OXFORD; 6b. OFFICE SYMBOL (If applicable): M1C	7a. NAME OF MONITORING ORGANIZATION: AFOSR/NA
6c. ADDRESS (City, State and ZIP Code): Parks Road, Oxford OX1 3PJ, UK	7b. ADDRESS (City, State and ZIP Code): Bolling AFB, D.C. 20332
8a. NAME OF FUNDING/SPONSORING ORGANIZATION: AIR FORCE OFFICE OF SCIENTIFIC RESEARCH; 8b. OFFICE SYMBOL (If applicable): NA	9. PROCUREMENT INSTRUMENT IDENTIFICATION NUMBER: AFOSR-82-0346
8c. ADDRESS (City, State and ZIP Code): BOLLING AFB DC 20332-6448	10. SOURCE OF FUNDING NOS.

PROGRAM ELEMENT NO.	PROJECT NO.	TASK NO	WORK UNIT NO
61102F	2307	B1	

11. TITLE (Include Security Classification): Behaviour of Fibre-Reinforced Composites under Dynamic Tension

12. PERSONAL AUTHOR(S): K Saka and J Harding

13a. TYPE OF REPORT	13b. TIME COVERED	14. DATE OF REPORT (Yr., Mo., Day)	15. PAGE COUNT
Final	FROM 30.9.82 TO 14.3.84	1984, August	51

16. SUPPLEMENTARY NOTATION

17 COSATI CODES		
FIELD	GROUP	SUB. GR.

18. SUBJECT TERMS (Continue on reverse if necessary and identify by block number):
Fibre-reinforced composites
Tensile impact testing
Hopkinson-bar tests

19. ABSTRACT (Continue on reverse if necessary and identify by block number):

A small gas gun, capable of accelerating a projectile 1m long by 25.4mm dia. to about 50m/s, and an extended split Hopkinson pressure bar apparatus have been designed and constructed for the tensile impact testing of fibre-reinforced composite specimens at strain rates of the order of 1000/s. Commissioning tests have shown equilibrum in the specimen to be attained at an early stage in the test and the effects of stress wave reflections in the specimen grip regions on the calculated stress-strain response to be negligibly small.

A technique has been developed for the preparation of low volume fraction 'model' hybrid specimens, unidirectionally reinforced with a single layer of fibre tows, alternately of glass and of carbon fibres. Specimens have also been prepared from commercially supplied carbon/glass and carbon/kevlar epoxy plates with different stacking sequences for the carbon and glass or carbon and kevlar reinforcing mats to allow specimens with a range of hybrid fractions.

(Continued on reverse)

20. DISTRIBUTION/AVAILABILITY OF ABSTRACT	21. ABSTRACT SECURITY CLASSIFICATION
UNCLASSIFIED/UNLIMITED ☒ SAME AS RPT. ☐ DTIC USERS ☐	Unclassified

22a. NAME OF RESPONSIBLE INDIVIDUAL	22b. TELEPHONE NUMBER (Include Area Code)	22c. OFFICE SYMBOL
ANTHONY K AMOS	(202) 767-4937	AFOSR/NA

DD FORM 1473, 83 APR EDITION OF 1 JAN 73 IS OBSOLETE.

UNCLASSIFIED

SECURITY CLASSIFICATION OF THIS PAGE

19. Abstract

In initial impact tests on the 'model' specimens tensile failures were obtained but with a trend for fracture close to the specimen/loading bar interface rather than in the centre of the parallel gauge section. Even so, a marked increase in fracture strength with strain rate was observed. Initial tests have also been performed on the woven reinforced carbon/glass hybrid specimens and the effect of hybrid fraction on the tensile modulus, fracture strength and fracture strain under impact loading has been determined. A preliminary study of the failure processes using optical and scanning electron microscopy has been undertaken.

PREFACE

Although classified as a 'Final' Report, the present document describes only the first stages of an investigation into the mechanical properties of carbon-glass and carbon-kevlar fibre reinforced composites under tensile impact loading. The original grant, no. AFOSR-82-0346, was for an initial one-year period, allowing a start to be made on the experimental programme. It was always anticipated, however, that further support would be needed. In the event, following the initial one-year period, two subsequent no cost extensions, totalling a period of 5½ months, also covered by this report, were required before further financial support became available on a new grant, no. AFOSR-84-0092. The work described in this present report, therefore, is continuing under the new grant.

CONTENTS

1. INTRODUCTION

The research programme, of which this report describes the first stage, arose from earlier work in which the tensile impact loading technique was developed (1) and results were obtained for the effect of tensile loading rate on the deformation and fracture of several different fibre reinforced composite materials (2,3). In the earlier work the impact testing machine used was a modification of one previously developed for the testing of isotropic metal specimens. The physical dimensions of that machine limited a full analysis of results obtained in tests on composite specimens to those which failed in times $\lesssim 30$ μs. The first object of the present work, therefore, was the construction of an extended impact loading machine operating on the same principles but allowing the full analysis to be performed at times up to 150 μs. Also involved was the construction of a new gas gun and the development of an improved electronic recording system employing transient recorders and, in the longer term, microcomputer processing of the test data.

The experimental programme called for the testing of two types of specimen, so-called 'model' specimens of low volume fraction, prepared within the Engineering Department at Oxford, and specimens of higher volume fraction also prepared at Oxford, from laminates supplied commercially by Fothergill and Harvey Ltd. Because of difficulties experienced in obtaining true tensile failures in unidirectionally-reinforced glass fibre composites of higher volume fraction under impact loading, for the first stages of the present programme, a woven reinforcement geometry was chosen for the commercially supplied specimens. The preparation of both types of specimen is described in section 3 of this report.

Initial tests were performed both on several model specimens and on one made from a fine weave glass-epoxy composite previously tested in the earlier work (2), where a full analysis of the specimen response was not possible. In the present tests this material is used to check the validity of the assumptions made in the earlier incomplete data analysis for such specimens. Subsequently, following the supply of the higher volume fraction carbon-glass and carbon-kevlar hybrid plates with a woven reinforcement geometry, specimens were cut and an initial set of tests performed at impact rates on specimens with five different combinations of reinforcement, all carbon, all glass, and three different ratios of carbon to glass. A discussion of these preliminary results forms the final section of this report.

---

(1) Harding. J. and Welsh, L.M., "Impact Testing of Fibre-Reinforced Composite Materials", 4th. Int. Conf. on Composite Materials, Tokyo, October 1982, (Japan Society for Composite Materials).

(2) Harding, J. and Welsh, L.M., "A Tensile Testing Technique for Fibre Reinforced Composites at Impact Rates of Strain", J. Mat. Sci., 18, 1810 - 1826, 1983

(3) Welsh, L.M. and Harding, J., "Effect of Strain Rate on the Tensile Failure of Woven Reinforced Polyester Resin Composites", to appear in the Proc. 3rd. Oxford Conf. on Mech. Props. Mat. at High Rates of Strain, Oxford, April 1984 (Institute of Physics, London and Bristol).

2. TESING EQUIPMENT

2.1 Gas Gun

The design of the gas gun is shown schematically in fig. 1 and a photograph of the gun is given in fig. 2. The projectile, an alloy steel bar 1m long by 25.4mm diameter, is carried on teflon guides in a mild steel barrel of 38.5mm internal diameter by 1.775m long. Initially valves A and B are closed and valve C, which vents to the atmosphere, is open. The projectile is loaded into the barrel and seals the reservoir at the H-ring pressure seals. The three valves, A, B and C are operated electromagnetically. Valve A is opened and the reservoir filled with nitrogen gas to a predetermined pressure. Valves A and C are then closed and the impact initiated by opening valve B which increases the pressure behind the projectile to that of the reservoir, causing it to move down the barrel until its back end clears the first H-ring seal whereupon the whole mass of gas in the reservoir becomes available to accelerate it. At the exit end of the barrel two photocells, a fixed distance apart, are used to check the projectile velocity just before impact with the test equipment occurs. A calibration curve relating projectile velocity to reservoir pressure is given in fig. 3.

2.2 Tensile Impact Apparatus

A modified tensile Hopkinson bar apparatus is used to convert the compressive impact of the projectile to a tensile loading wave in the specimen. In principle the design is identical to that previously described (1) and shown here in fig. 4. By extending the lengths of the instrumented input and the inertia bars to 451mm and 422mm respectively, the critical time delay, $T_2 - T_1$, for the analysis of the input bar traces is increased to ~ 142 μs and the corresponding analysis time for the output bar trace to 150 μs. A new weighbar tube was required and was constructed from 27mm diameter centreless ground annealed I.M.I. 318 titanium alloy bar, bored to a diameter of 3/8 in $\left\{\begin{matrix}+ 0.001 \text{ in} \\ + 0.003 \text{ in}\end{matrix}\right\}$ along its full length of 0.91m with a clearance diameter of 9/16 in at one end. An accurately straight bore is required since on this depends the alignment of the loading bars. The impact end of the weighbar tube is closed with a solid bar of the same material, the impact head, against which the projectile impinges. At the further end a yoke, also of annealed IMI 318 titanium alloy bar, connects the weighbar tube with the input loading bar, reflecting the compressive loading wave in the former as a tensile loading wave in the latter.

2.3 Electronic Recording Equipment

Strain gauges at stations I and II on the input bar, see fig. 4, monitor the incident and reflected stress waves on the input side of the specimen while strain gauges at station III on the output, or inertia bar, side monitor the stress wave transmitted through the specimen.

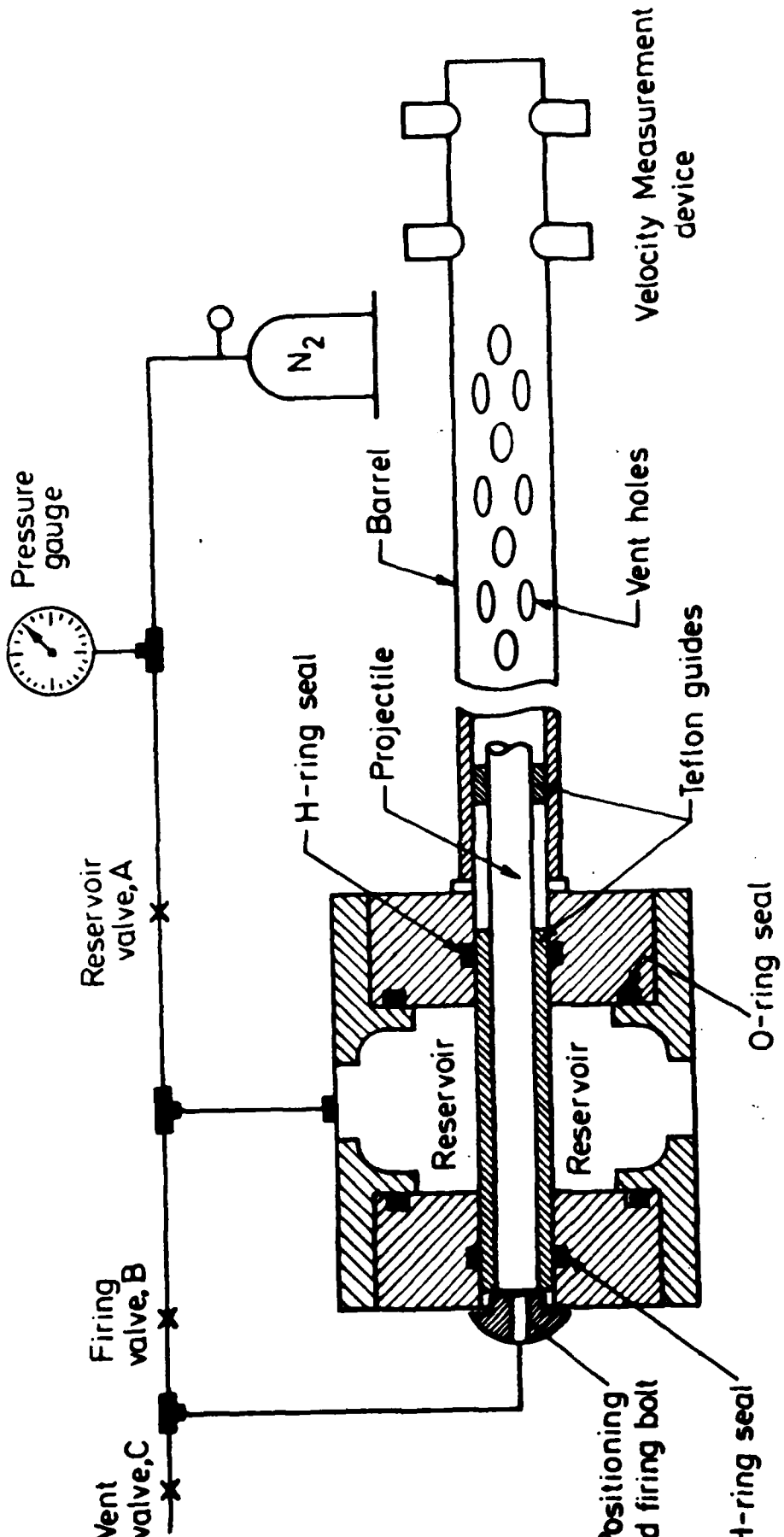

Fig.1 SCHEMATIC ARRANGEMENT FOR GAS-GUN

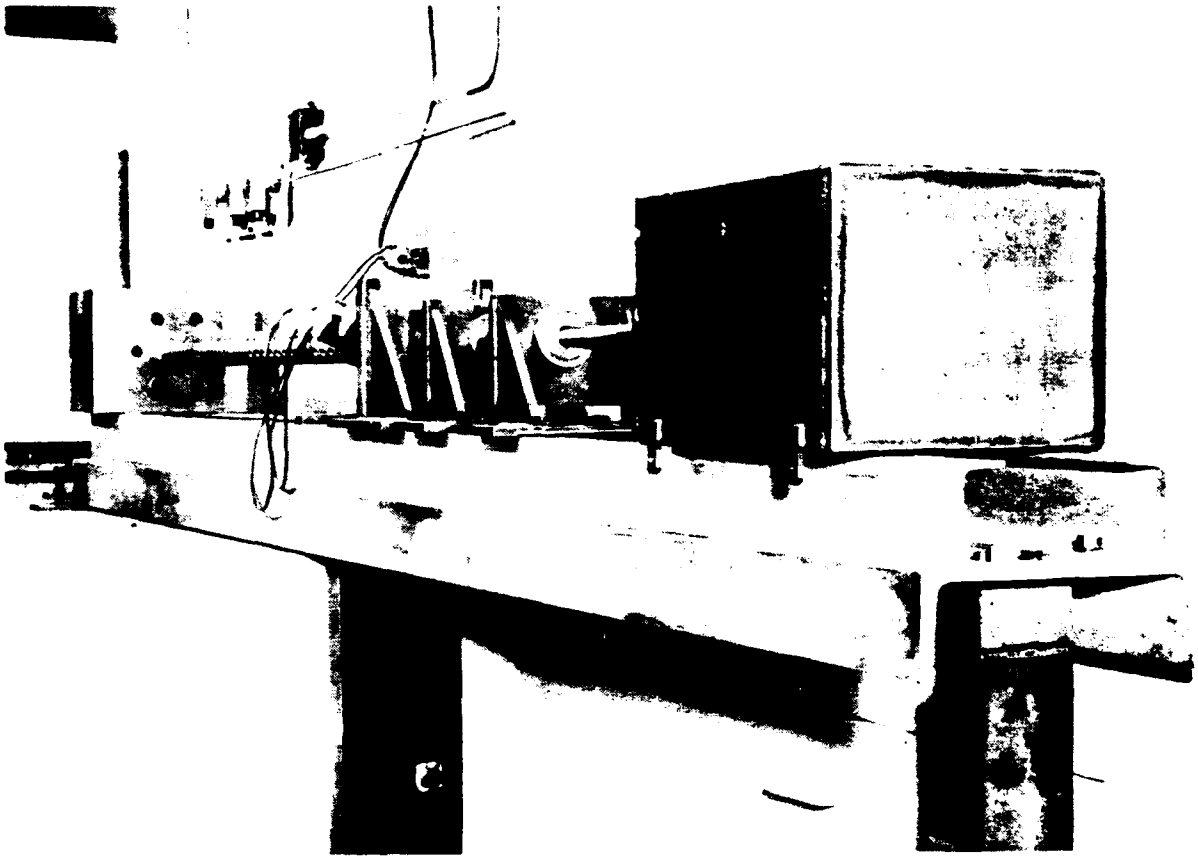

Fig.2 GENERAL VIEW OF GAS-GUN

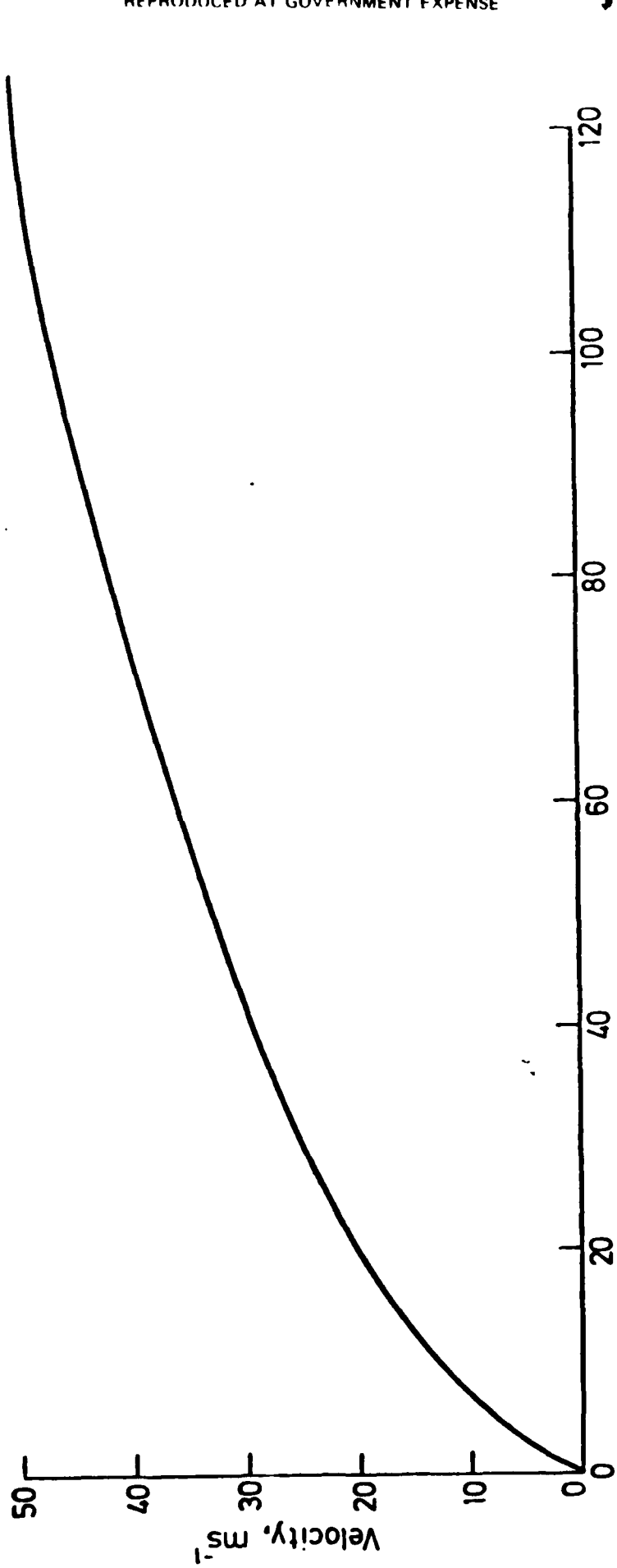

Fig.3 PRESSURE-VELOCITY CALIBRATION FOR GAS-GUN

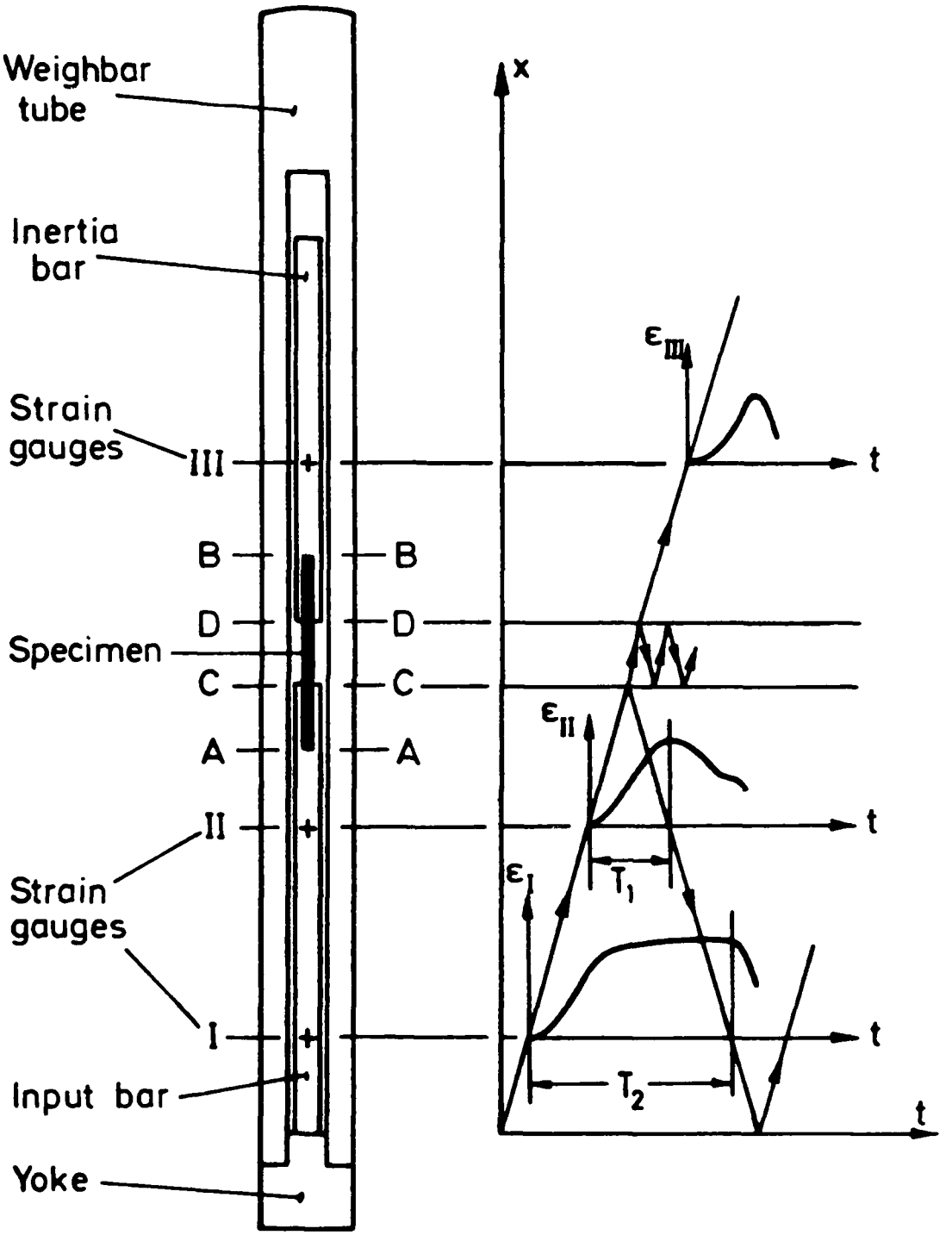

Fig.4 SCHEMATIC ARRANGEMENT AND LAGRANGE (x,t) DIAGRAM FOR TENSILE HOPKINSON-BAR

A set of such traces for a test at an impact velocity of about 11 m/s on a fine-weave glass-reinforced epoxy specimen with its axis of loading in the plane of reinforcement and at 45° to each of the directions of weave is shown in fig. 5. The total sweep time is 400 μs for each trace and calibration steps corresponding to output voltages from the strain gauge bridge of 10 mv, for gauge stations I and II, and 5 mv for gauge station III, are also recorded. The traces were originally obtained on two Datalabs type 922 dual channel transient recorders and were subsequently displayed on an oscilloscope and plotted on graph paper for manual calculation using an X-Y chart recorder. An interface between the transient recorders and a Rainbow micro-computer is currently being developed and a program is being written to permit computer analysis of the test data. The transient recorders are triggered externally using a delay unit and a trigger signal obtained when contact is made at the impact surface between the projectile and the weigh-bar tube impact head. In some specimen tests it is planned that strain gauges directly attached to the parallel gauge section of the specimen will be used to monitor specimen strain independently of the Hopkinson-bar analysis. A block diagram of the electrical recording system is shown in fig. 6.

3. SPECIMEN DESIGN

Thin strip specimens waisted in the thickness direction, as recommended for the quasi-static testing of unidirectionally-reinforced CFRP specimens (Ewins 4), were found in the earlier work (1, 2, 3) to give satisfactory results under tensile impact loading. Specimens of very similar geometry, therefore, were used for both types of test in the present investigation.

3.1 Model Specimens

A technique has been developed for preparing single-layer low volume fraction unidirectionally reinforced carbon/glass hybrid specimens to the general dimensions shown in fig. 7. Alternate fibre tows of carbon and glass were clamped in a specially designed mould and cast in epoxy resin, see fig. 8, using a modification of a technique developed by Welsh (5). Here, however, because of the difference in thickness between the carbon and the glass fibre tows, to maintain alignment across the mould it was necessary to clamp each fibre tow individually. To ensure that the single layer of fibre tows were accurately aligned along the centre-line of the final specimen, the bottom surface of the mould was taken as a reference surface for one side of the specimen, see fig. 8. The slots, within which the fibre tows are spaced, were then carefully machined to a depth which allowed the centre-line of the fibre tows to lie exactly half the total specimen thickness above the bottom of the mould.

Prior to the laying of the fibres, a silicone mould release agent (Dow Corning Compound no. 7) is baked into the mould at about 120°C. After baking, a thin layer of Ciba-Geigy mould release QZ13 is applied to the mould. The technique for casting hybrid model specimens was developed and the first specimens were prepared using the same resin system and the same reinforcing fibres as had been used in the earlier work (5). The resin consisted of 100 parts by volume of Ciba-Geigy MY750, a liquid epoxy of medium viscosity, 100 parts by volume of Hardener HY905 and 2 parts by volume of Accelerator DY063 (triamylammonium phenate).

To mix the components, the liquid MY750 is heated to 30°C and held at this temperature for 20 minutes. The hardener, followed by the accelerator, are then added with thorough stirring in each case. The resulting mixture is then raised to 60°C and held at that temperature for 20 minutes. The mould is prewarmed to 60°C with the fibres in place. The liquid resin is then poured over a glass rod into the centre part of the mould, during which time the temperature falls to about 55°C. The mould is replaced in the oven and heated to 120°C at a rate of 1°C/minute.

---

(4) Ewins, P.D., "Tensile and Compressive Test Specimens for Unidirectional Carbon Fibre Reinforced Plastics", R.A.E. Technical Report No. 71217, 1971.

(5) Welsh, L.M., Oxford University Engineering Department (unpublished work)

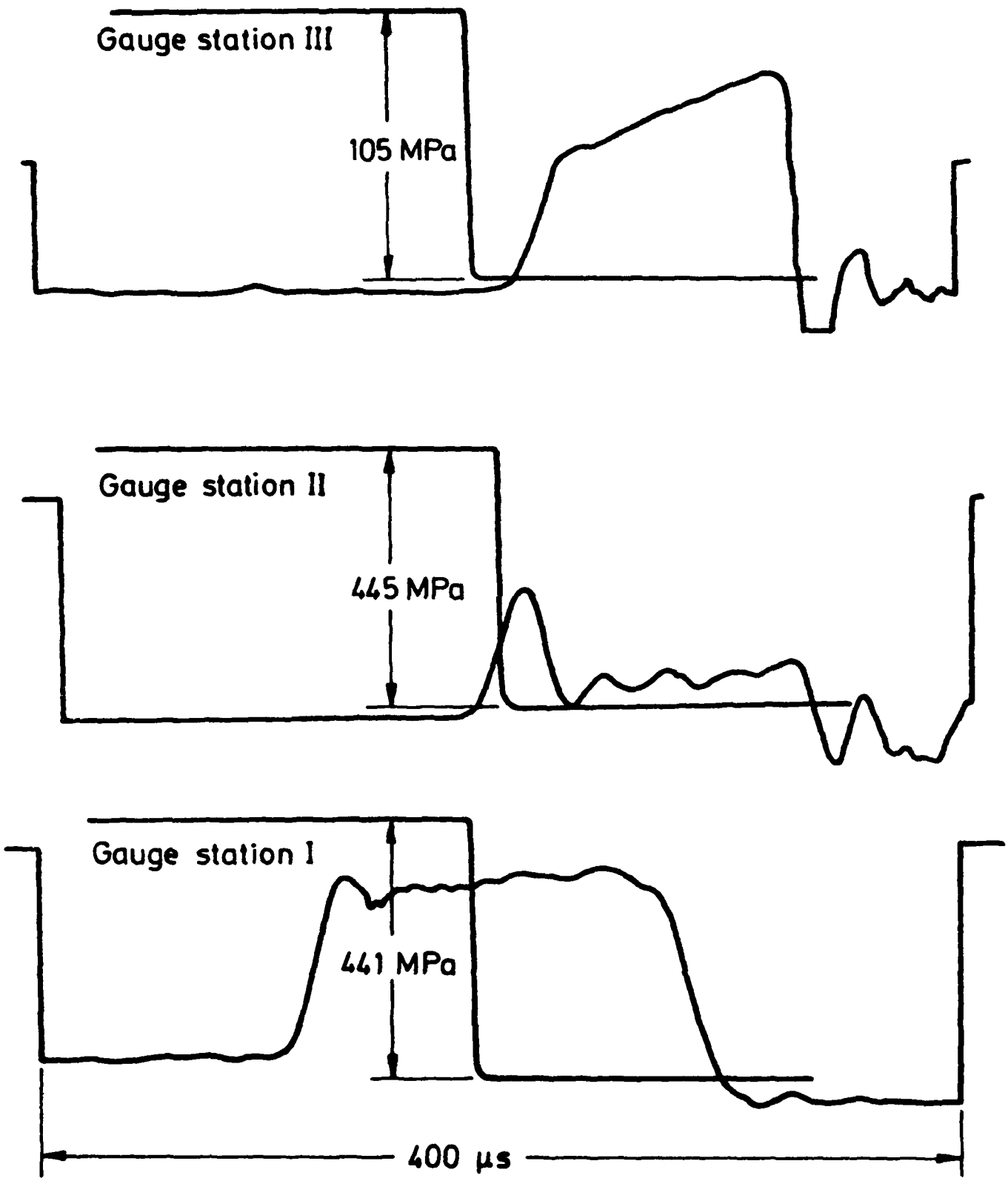

Fig.5 STRAIN-GAUGE SIGNALS FOR CALIBRATION TEST ON GFRP SPECIMEN

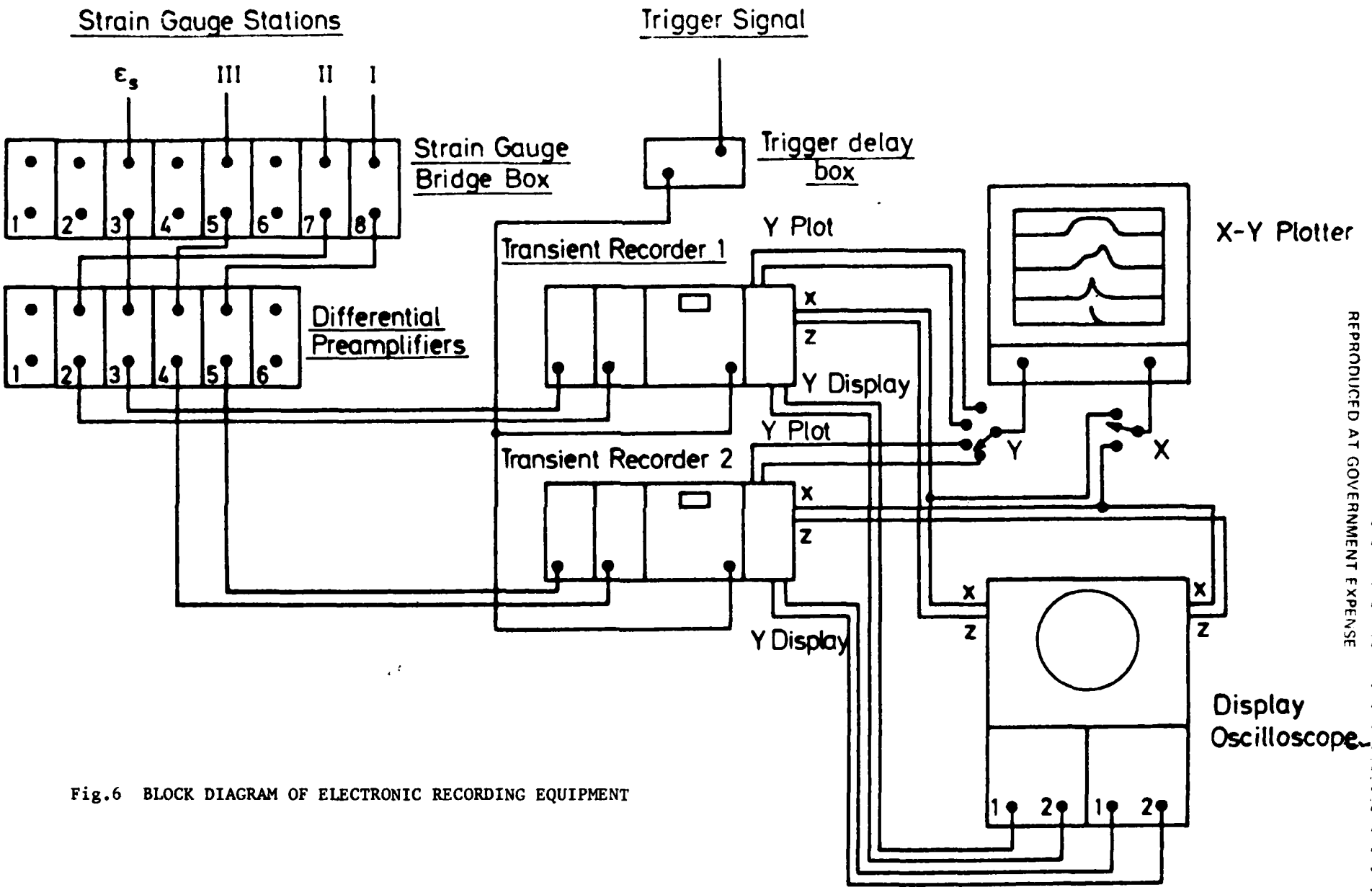

Fig.6 BLOCK DIAGRAM OF ELECTRONIC RECORDING EQUIPMENT

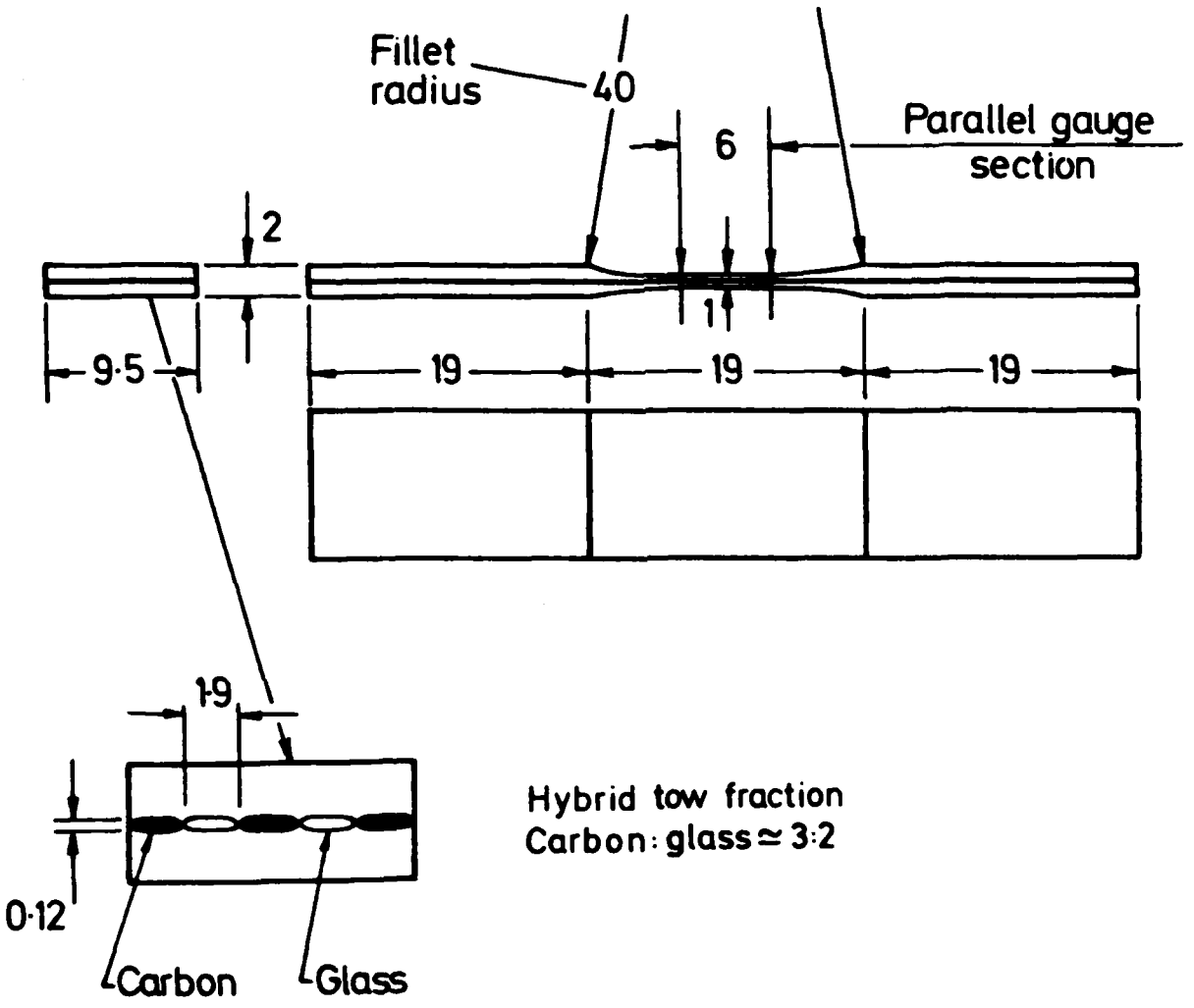

Fig.7 DESIGN OF MODEL SPECIMENS

(all dimensions in mm)

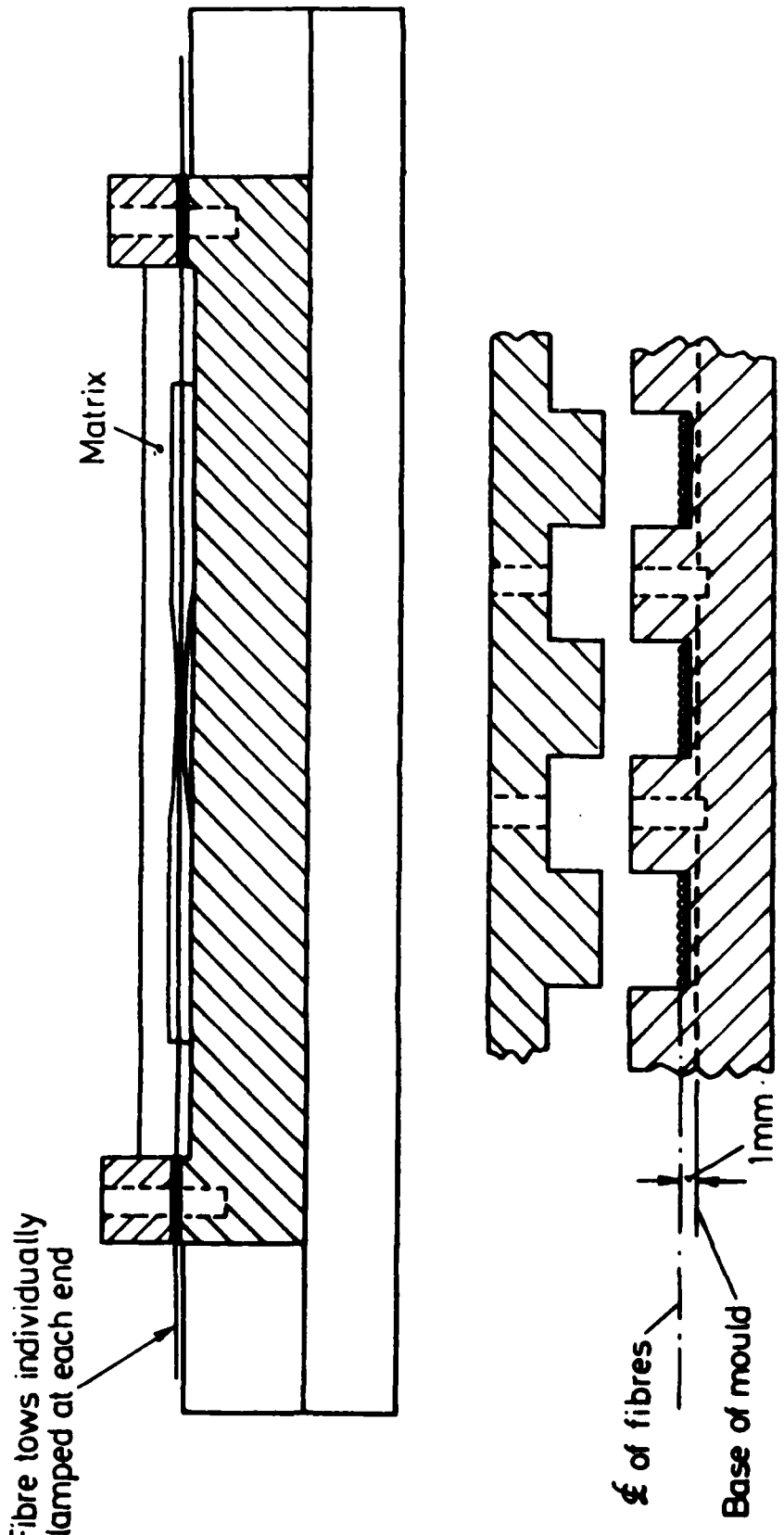

Fig.8 DESIGN OF MOULD FOR PREPARATION OF MODEL SPECIMENS

The oven door is then opened to allow the mould to cool down to room temperature. No problems were experienced in wetting the fibres. As an experiment a solution of the resin in acetone was used on one occasion to wet the fibres but it was difficult to avoid damage to the fibres and to maintain their alignment so the practice was discontinued.

The carbon and glass fibre tows used to reinforce the model specimens were taken from a hybrid fabric supplied by Bristol Composites Ltd. and designated Hyfil-Torayca Z tape-01. It consisted of alternate rows of continuous 600 tex E-glass fibre tows and 6000 filament Hyfil-Torayca 130C carbon fibre tows. The mould was designed to allow the preparation of 10 specimens from each cast plate so that a complete set of three tests at each of three loading rates, low, intermediate and impact, could be performed on specimens cut from the same casting. During initial development of the moulding technique, however, each plate contained specimens with a variety of reinforcement configurations, from all glass to all carbon, and, as yet, no tests have been performed at the intermediate rate and only one at the quasi-static rate.

3.2 Commercial Woven Reinforced Specimens

Seven laminated composite plates, each 0.3m square and of 2mm nominal thickness, were supplied by Fothergill and Harvey Ltd. All laminates were hand laid up using the Ciba-Geigy XD 927 epoxy resin system, with 100 parts by weight of resin to 36 parts by weight of hardener, and a cure schedule of 24 hours at room temperature followed by 16 hours at 100°C. Three plates were, i) all carbon to an actual thickness of 3.4mm and containing 12 woven mats (plies) with, overall, a 50% fibre content by weight, ii) all glass to an actual thickness of 1.75mm and containing 14 plies, also with, overall, a 50% fibre content by weight, and iii) all kevlar to an actual thickness of 2.14mm and containing 18 plies with, overall, a 35% fibre content by weight.

All fabrics were of a plain weave construction. The carbon fibre fabric was woven from Toray 3000 filament fibre tows, type T300-3000A, and had a weight of 189g/m^2 and an approximate thickness of 0.28mm. The fibres were supplied with a surface treatment suitable for use with epoxy resin. Unfortunately this fabric has a relatively coarse weave geometry, with only 47 ends and picks per 10cm. Previous work (3) has shown that more reliable results are obtained at impact rates when the scale of the reinforcement geometry is relatively fine in comparison with the overall specimen dimensions. However, to obtain a finer weave would have required the use of 1000 filament fibre tows and the production of specially woven fabrics which would have been extremely expensive. The glass fabric was woven from continuous E-glass fibres, designation 11 x 2EC5, and had a weight of 96g/m^2 and an approximate thickness of 0.08mm. With 252 ends and 173 picks per 10cm the weave was much finer than for the carbon fabric. The fibre finish, type 205, was suitable for use with both epoxy and polyester resins. The kevlar fabric was woven from fibres with a tex of 21.7 and a surface finish, type 286, also suitable for use with both epoxy and polyester resins. The fabric had a weight of 60g/m^2 and an approximate thickness of 0.11mm. With 134 ends and picks per 10cm the weave geometry was relatively fine.

The remaining four laminated plates were of hybrid construction, either alternating layers of carbon and glass or carbon and kevlar, one plate of each, or two layers of glass or kevlar alternating with a single layer of carbon, also one plate of each. In each case the overall fabric weight fraction was 50%. In addition to the seven commercially supplied laminates a plate of unreinforced XD 927 epoxy resin has been prepared, using a steel mould. Large distortions of the plate were avoided by carefully following the recommended cure schedule, 24 hours at room temperature followed by 16 hours at 100°C, after which the mould was removed from the oven to cool in air. Subsequent examination under polarised light revealed stress concentrations throughout the length of the plate. These were removed by an annealing treatment in which the plate was held at just over the cure temperature for 24 hours and then cooled to room temperature at a rate of 10°C/hour or less. All stress concentrations were removed by this treatment. It is possible, of course, that if the cooling rate had been controlled in this way after the initial cure, the subsequent annealing treatment would not have been necessary.

Specimens were cut from the laminates to the standard dimensions, for the various carbon/glass hybrids, given in fig. 9. The specimen thickness in the parallel gauge section and in the thicker grip sections varied with the reinforcement configuration as shown in fig. 9 for three different carbon to glass hybrid weight fractions and for the all-glass and the all-carbon specimen configurations. The thickness in the grip sections is approximately twice that in the gauge section. Specimens were cut using specially designed jigs and were carefully surface finished by hand.

Originally it had been hoped to include tests on composite laminates reinforced with similar layers of hybrid fabric mats, each mat woven from alternating tows of carbon and glass or carbon and kevlar. Unfortunately, the only hybrid fabrics available were unsuitable and the production of specially woven fabrics would again have been extremely expensive.

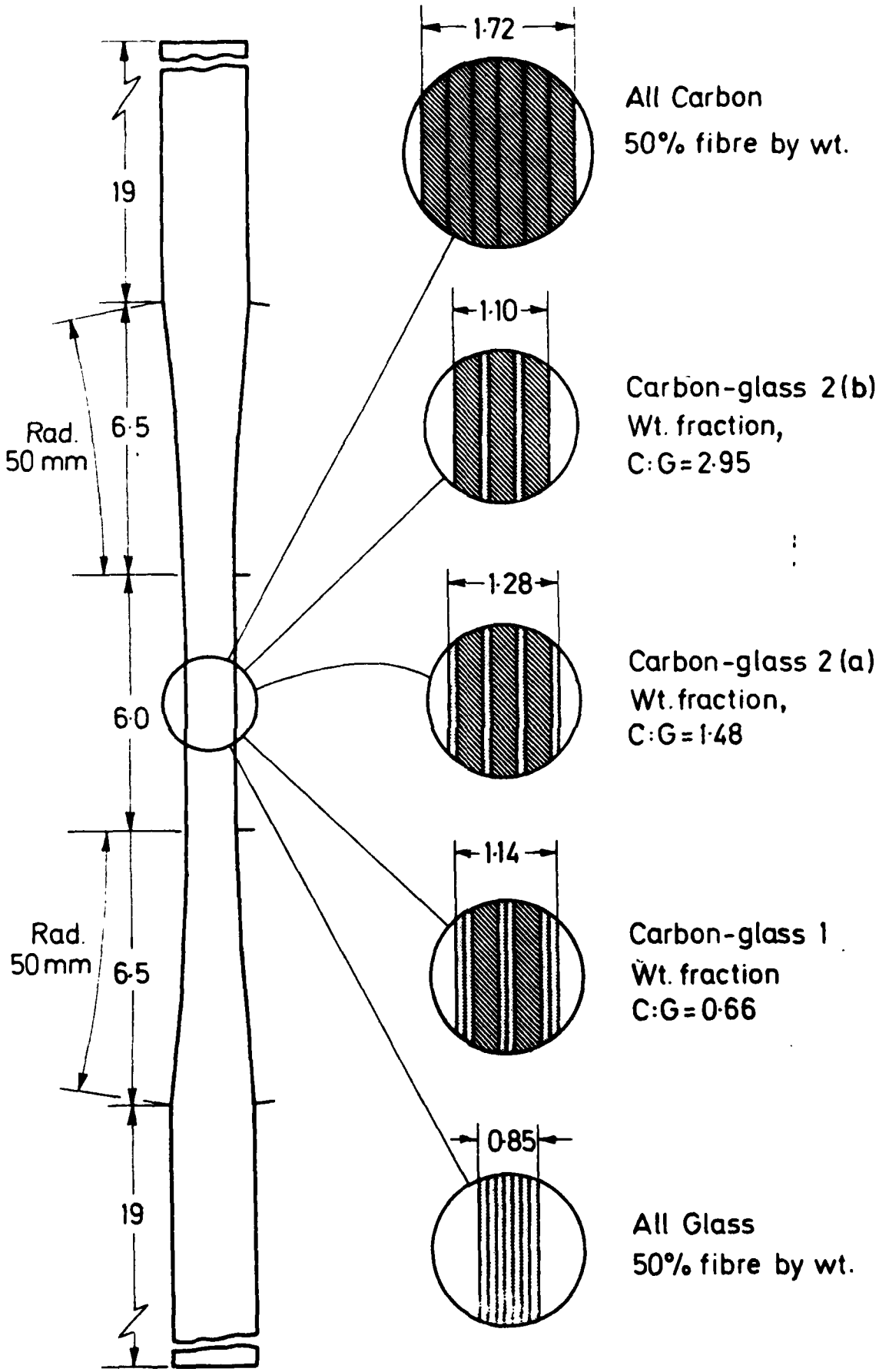

Fig.9 DESIGN OF CARBON/GLASS WOVEN REINFORCED SPECIMENS

4. ANALYSIS OF IMPACT TEST DATA

4.1 Approximate Analysis

In previous work on unidirectionally-reinforced CFRP specimens using the experimental configuration of fig. 4, the strain-time signals from gauge stations, I, II and III, when subjected to the standard Hopkinson bar analysis, gave the results shown in fig. 10. Exceptionally good agreement was obtained between the stress levels, σ_{cc} and $E\varepsilon_{III}$, determined at the input and output ends of the specimen. Some allowance was made in this calculation for the modified wave speed in the grip regions of the loading bars, AA - CC and BB - DD in fig. 4, due to the presence of the composite but the change in impedance in these regions compared with that in the loading bars alone was so small, for this particular test material, that wave reflections at sections AA and BB were ignored. The almost identical profiles for the strain-time signals from gauge stations I and II at times up to T_1, see fig. 10, was further justification for this procedure.

In the present tests, however, using glass fibres and a woven reinforcement geometry where the expected specimen modulus is significantly lower and, in some cases, the thickness of the specimen in the grip region considerably greater, a more marked change in impedance across the sections at AA and BB might be expected. The worst case is likely to be for a woven glass reinforced epoxy composite tested in the 45° orientation where previous work suggests a modulus under impact loading of about 18 GPa, compared with about 140 GPa for the unidirectionally reinforced CFRP, and where the specimen thickness in the grip regions was 3.4mm, compared with 2mm for the previous CFRP tests. The corresponding impedance mismatch at AA could be expected to result in a reflected wave equal in magnitude to about 20% of the incident wave, while at BB a transmitted wave some 20% greater than the incident wave might be anticipated. No evidence for such reflections, however, was apparent when comparing the rising profiles of the signals from gauge stations I and II in the test of fig. 5. As shown in fig. 11, these remain coincident for times $\leq T_1$. While this is still on the steeply rising part of the curve, where a small difference in magnitude might be difficult to detect, reflections from section AA would be expected to show up as a divergence between the rising profiles at even earlier times,ie., at about T_1' rather than T_1.

Assuming that these reflections, if present, are small enough to be ignored, the stress variation at the input end of the specimen, σ_{cc}, is calculated from $E\varepsilon_I$ and $E\varepsilon_{II}$ in the normal way and is shown as the dotted curve in fig. 11. It is compared with the stress at the output end of the specimen, $E\varepsilon_{III}$, shown chain-dotted in fig. 11, where t_s is the estimated transit time for a stress wave across the specimen, ie., from CC to DD.

Although in general form the stress variations at the input and the output ends of the specimen are similar, the almost exact agreement found previously, see fig. 10, is not reproduced here. The present results show as good a correlation as would normally be expected in tensile impact testing where the input stress, σ_{cc}, can only be determined with limited accuracy as the small difference between a large incident and a large reflected wave. For this reason, it is usual to base specimen stress measurements on the directly determined output stress levels, $E\varepsilon_{III}$. It may perhaps be noted that in the earlier work on unidirectionally-reinforced CFRP the specimens were much stronger and the reflected wave correspondingly much smaller, allowing a more accurate determination of σ_{cc}. Also the divergence between $E\varepsilon_I$ and $E\varepsilon_{II}$ at $t=T_1$ occurred at a later time, close to the end of the rising profile of $E\varepsilon_{II}$, further improving the accuracy of the wave analysis.

The effect of relating the specimen stress entirely to the output signal, $E\varepsilon_{III}$, rather than to the mean of both the output and the input stresses, ie., σ_m given by

$$\sigma_m = \tfrac{1}{2}(\sigma_{cc} + E\varepsilon_{III})$$

is shown in fig. 12, where the two resulting stress-strain curves are compared. That based on $E\varepsilon_{III}$ agrees very closely with previous results for the same material (2) at a similar strain rate, about 900/s in the present tests. While there is little difficulty in discounting the dashed curve, based on σ_m, at strains greater than about 2%, because of the difficulties involved in accurately determining σ_{cc}, and hence σ_m, a problem still remains regarding the confidence with which the initial modulus value can be determined. This is particularly important for composite specimens where fracture at strains as low as 2 to 3% is not unusual and the only significant parameters to be measured are the fracture strength and the modulus, both of which may well be rate-dependent. In the present tests a modulus of 17.8 GPa, based on $E\varepsilon_{III}$, at an average strain rate of 890/s compares with a previous measurement (2) of 18.3 GPa at about 1120/s. However, if the mean stress, σ_m, is used, an apparent modulus of 26.7 GPa is obtained. Since measurements made during the initial stages of stress wave loading are likely to be particularly sensitive to any reflections in the grip regions it was decided to repeat the analysis of fig. 11 making allowance for such reflections so as to assess, in particular, what effect they might have on the resulting value for the modulus.

4.2 Data Analysis including Stress-Wave Reflections in Grip Regions

Details of the analysis for the effect of reflections at AA and BB are given in the Appendix. The effective modulus and density in each grip region are estimated from the individual values for the composite specimen and the loading bar materials by application of the rule of mixtures. These values are then used to calculate a corresponding effective wave speed, c, and driving point impedance, $z = \rho cA$.

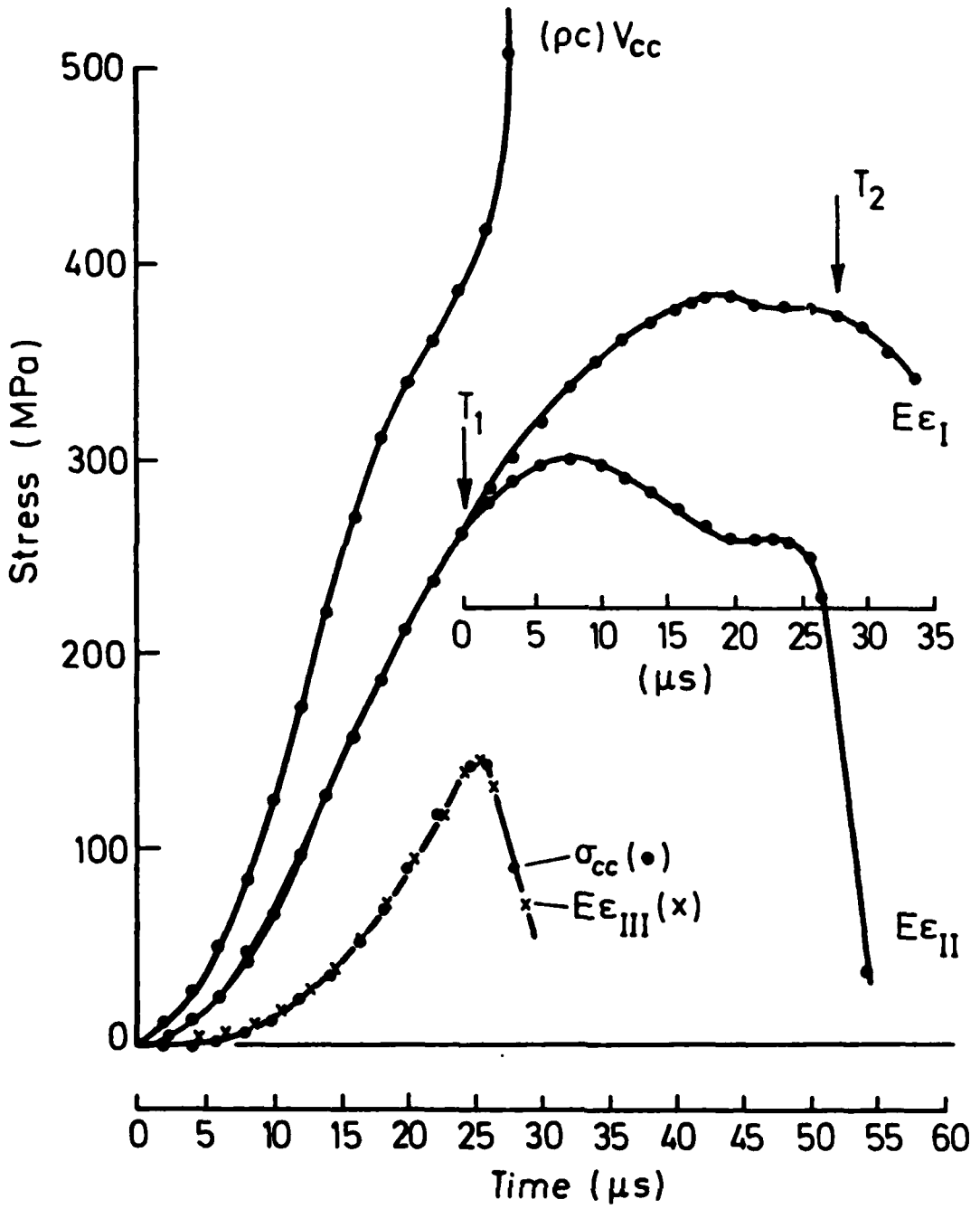

Fig.10 HOPKINSON-BAR ANALYSIS FOR UNIDIRECTIONALLY-REINFORCED CFRP SPECIMEN (from ref. 1)

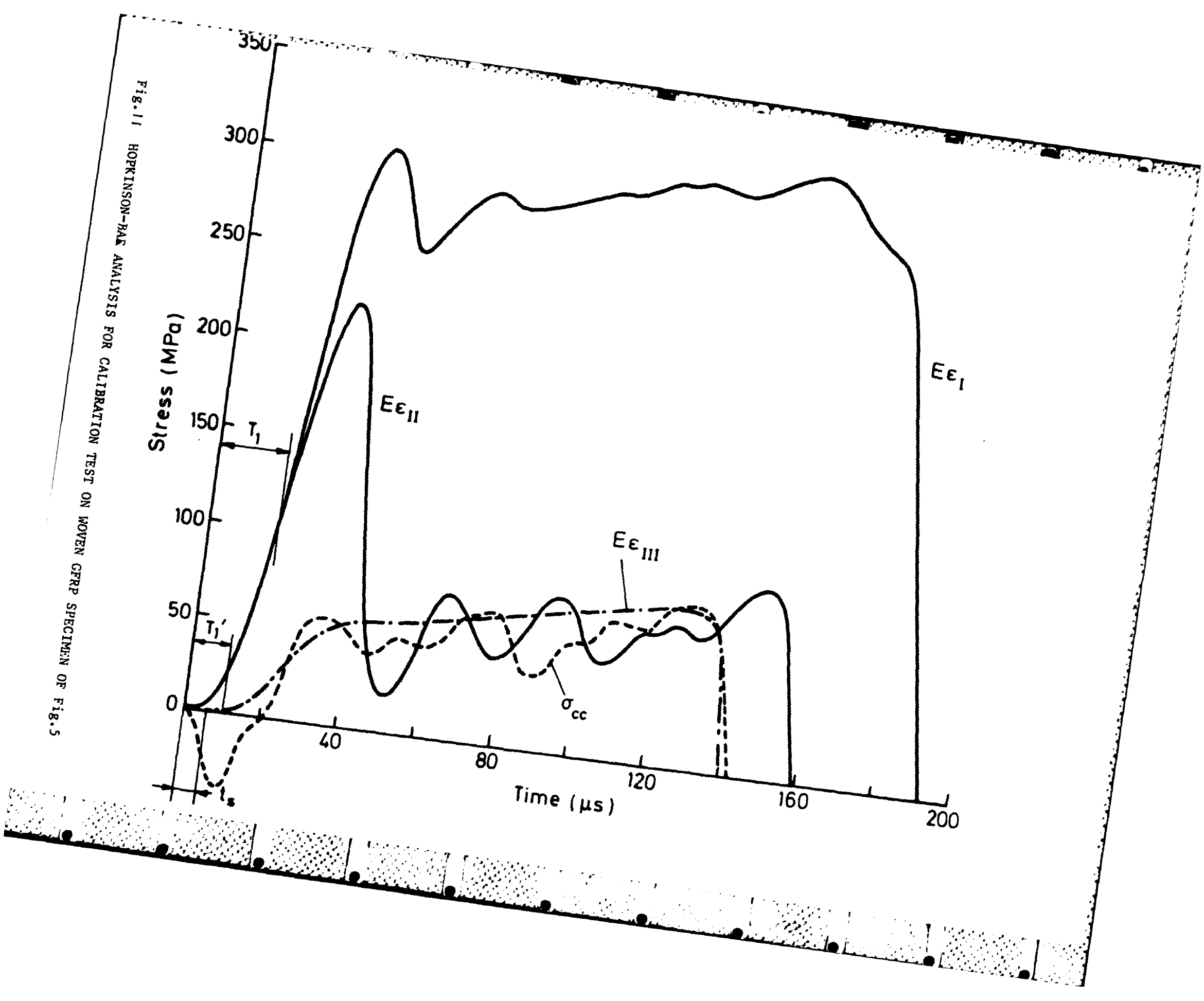

Fig.11 HOPKINSON-BAR ANALYSIS FOR CALIBRATION TEST ON WOVEN GFRP SPECIMEN OF Fig.5

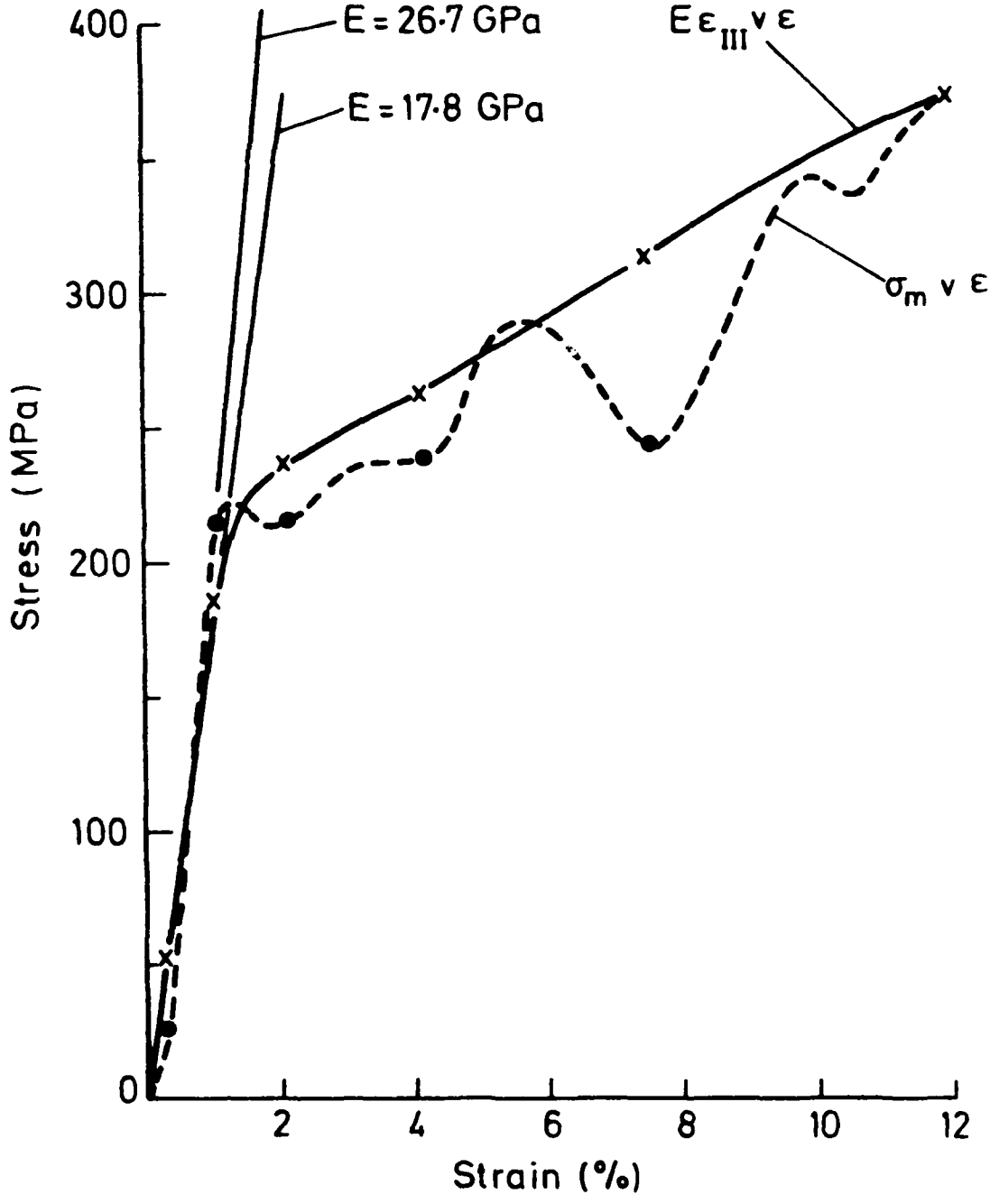

Fig.12 STRESS-STRAIN CURVES FOR CALIBRATION TEST, IGNORING WAVE REFLECTIONS IN SPECIMEN GRIP REGIONS
(x - based on output bar signal; • - based on specimen 'mean' stress)

The dynamic modulus of the composite has to be assumed and is estimated from the results of previous work. An approximate value is adequate as the calculation is not sensitive to small differences in modulus.

The results of this analysis are shown in figs. 13a and 13b where are compared, respectively, the stress at the input end of the specimen, σ_{cc}', after allowance for reflected waves at AA, with that previously calculated, σ_{cc}, and the stress at the output end of the specimen, σ_{DD}, after allowance for reflections at BB, with that previously assumed, $E\varepsilon_{III}$. The only significant difference in each case is, as suspected, in the rising profile, the rate of stress increase with time being slightly reduced. As shown in the corresponding dynamic stress-strain curves, given in fig. 14, this results in a slight decrease in the dynamic modulus, to 16.6 GPa, for the curve based on the output stress, σ_{DD}, while for the curve based on $\sigma_m = \frac{1}{2}(\sigma_{cc}' + \sigma_{DD})$ the modulus remained unaltered, within the accuracy with which it can be determined, at about 26.7 GPa. It is concluded that the marginal differences resulting from allowing for the reflections in the grip regions do not justify the complications of the analysis involved.

Nevertheless, in an attempt to improve the agreement between the calculated input and output stresses at each end of the specimen gauge length, it is proposed that further calibration tests be performed in which gauge station II is moved further away from the specimen, thus increasing the time T_1 in the hope that the divergence between the signals $E\varepsilon_I$ and $E\varepsilon_{II}$ will now be beyond the region of rapidly rising stress. In addition, strain gauges will be attached directly to the specimen parallel gauge section, as in previous work (1, 2), so as to allow the specimen strain to be checked independently of the Hopkinson-bar analysis over the linear elastic region of the stress-strain curve.

5. RESULTS AND DISCUSSION

Although these further calibration tests, described in section 4 above, are still to be completed, in order to obtain an initial indication of the mechanical response under tensile impact loading for the various composite materials described in section 3 a series of tests has been performed, as described below, and stress-strain curves derived, ignoring stress-reflections in the grip regions and relating specimen stress measurements directly to the output stress wave, $E\varepsilon_{III}$.

5.1 Commercial Woven Reinforced Specimens

Tests have been performed, at an impact velocity of about 11m/s, on the five types of woven-reinforced composite specimens illustrated in fig. 9, having either a) an all-carbon reinforcement or b) an all-glass reinforcement or c) one of the three carbon-glass hybrid fractions. In all tests a tensile failure was obtained with fracture across the central parallel gauge region of the specimen, as shown in fig. 15, for a test on a type 2a carbon/glass hybrid specimen.

The set of transient recorder stress-time traces for a test on an all-carbon specimen is shown in fig. 16 and the corresponding Hopkinson-bar analysis is given in fig. 17. This material has a much higher strength, more than twice that for the woven-glass specimen loaded in the 45^{o} direction, see figs. 11 and 12. Consequently, the magnitude of the reflected wave is reduced and the accuracy of the input stress (σ_{cc}) calculation is improved, leading to a much closer agreement with the output stress level ($E\varepsilon_{III}$), as evident in fig. 17. Although this agreement is still not quite as good as that reported previously it does increase confidence in the assumption that the output bar signal gives an adequate indication of the specimen stress during the course of the test, the apparent differences across the specimen being due, largely, to the difficulties of determining the input stress with sufficient accuracy.

The resulting dynamic stress-strain curve is shown in fig. 18 where is also given the variation of strain rate with strain during the course of the test. Over much of the test the strain rate lies between 600 and 800/s although the average strain rate, defined as the strain at fracture divided by the time to fracture, is lower at about 330/s. The specimen response is essentially linear elastic, with a modulus of 46.7 GPa, to a strain of about 1.2%. Beyond this some anelastic deformation is observed before the peak load is reached at 1.38% strain. This is followed, as may be seen from the gauge station III stress-time trace of fig. 16, by rapid unloading as the specimen fractures.

In analysing the traces of fig. 16 an arbitrary time zero is chosen for trace I and elementary one-dimensional longitudinal elastic wave theory is used to estimate the time delays between stations I, II and III and hence the corresponding time zero's for traces II and III.

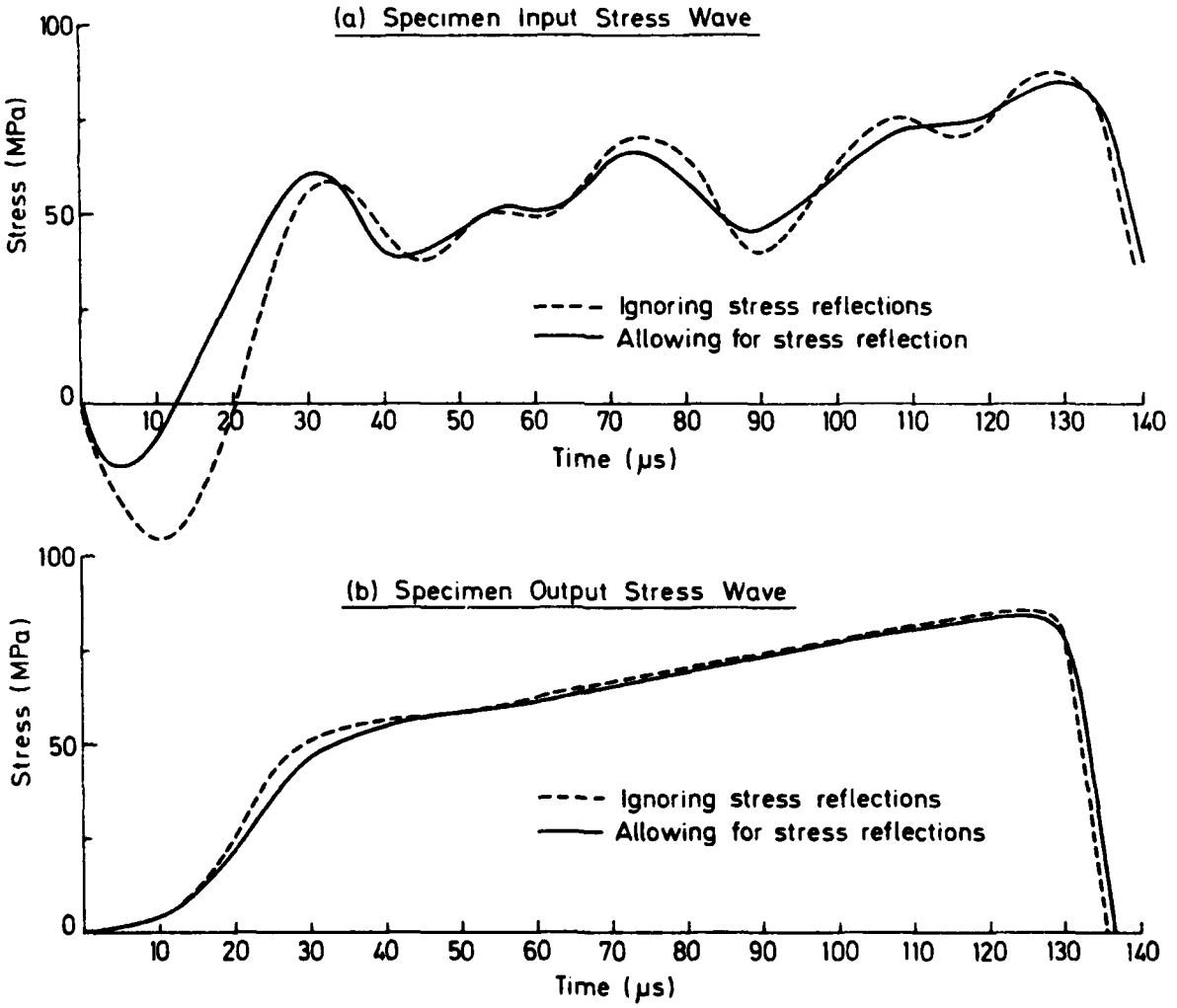

Fig.13 EFFECT OF CORRECTING FOR STRESS WAVE REFLECTIONS IN SPECIMEN GRIP REGIONS

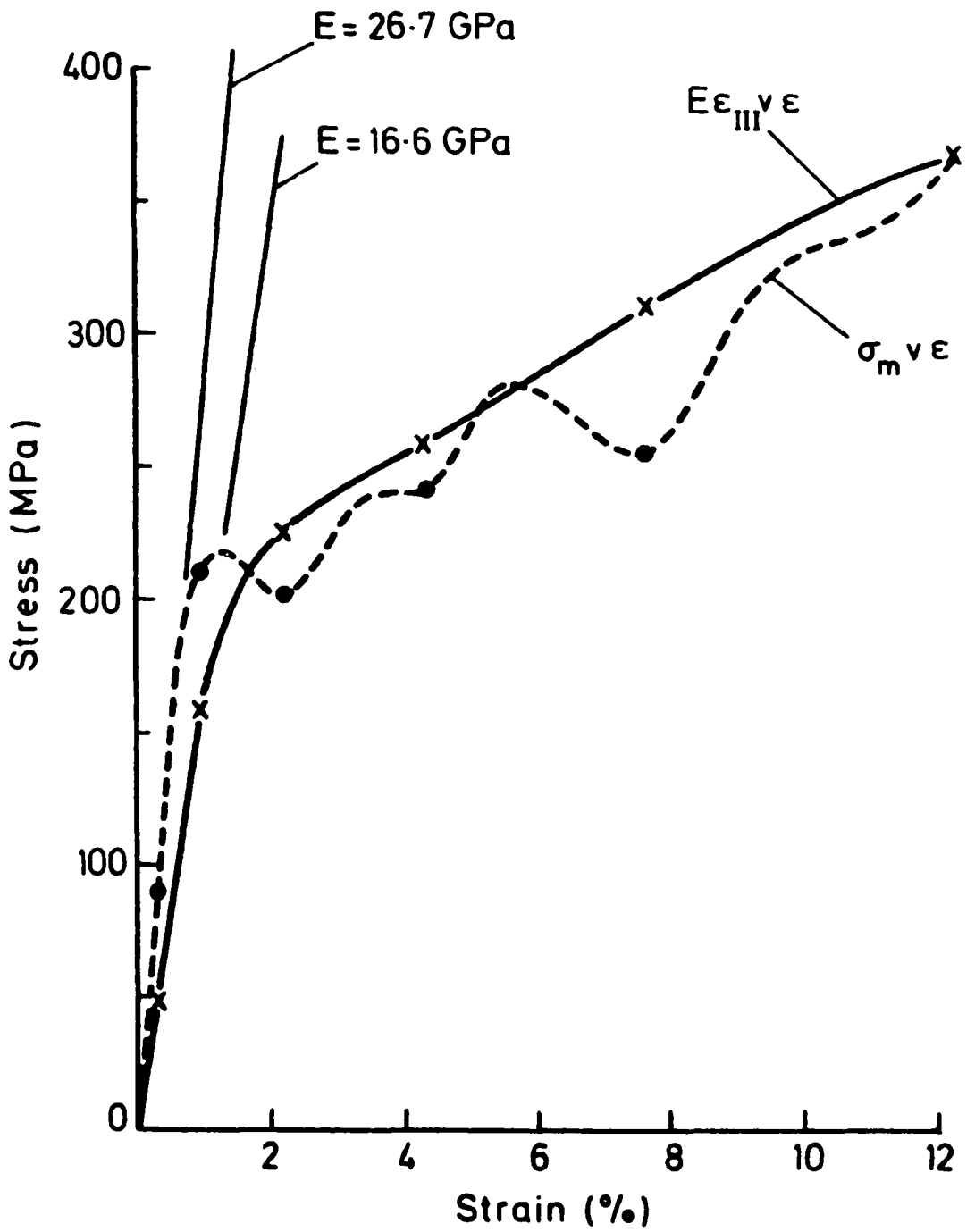

Fig.14 STRESS-STRAIN CURVES FOR CALIBRATION TEST, INCLUDING CORRECTION FOR STRESS WAVE REFLECTIONS IN SPECIMEN GRIP REGIONS
(x - based on output bar signal; • - based on specimen 'mean' stress)

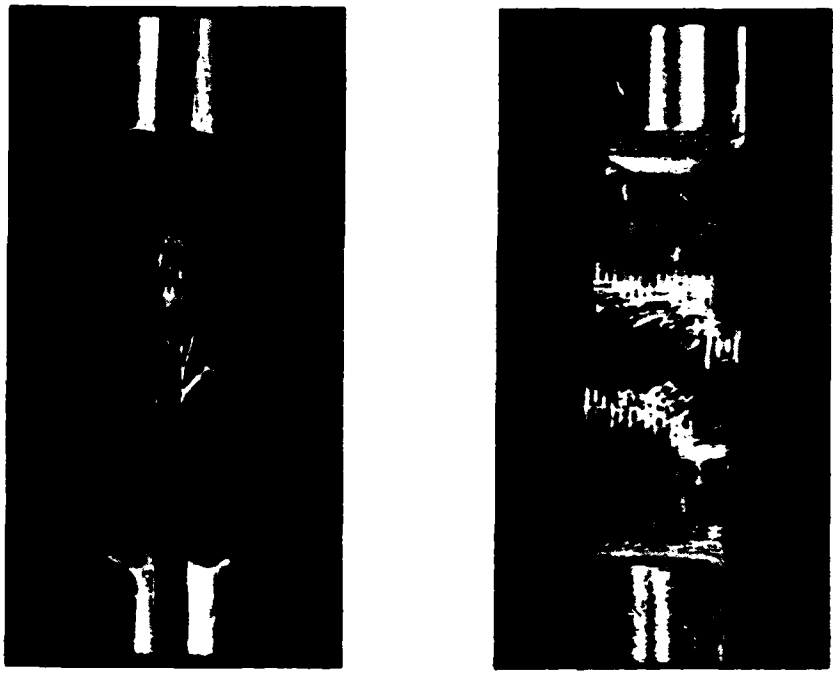

Fig.15 TENSILE FAILURE MODE IN AN IMPACTED TYPE 2a CARBON/GLASS HYBRID SPECIMEN

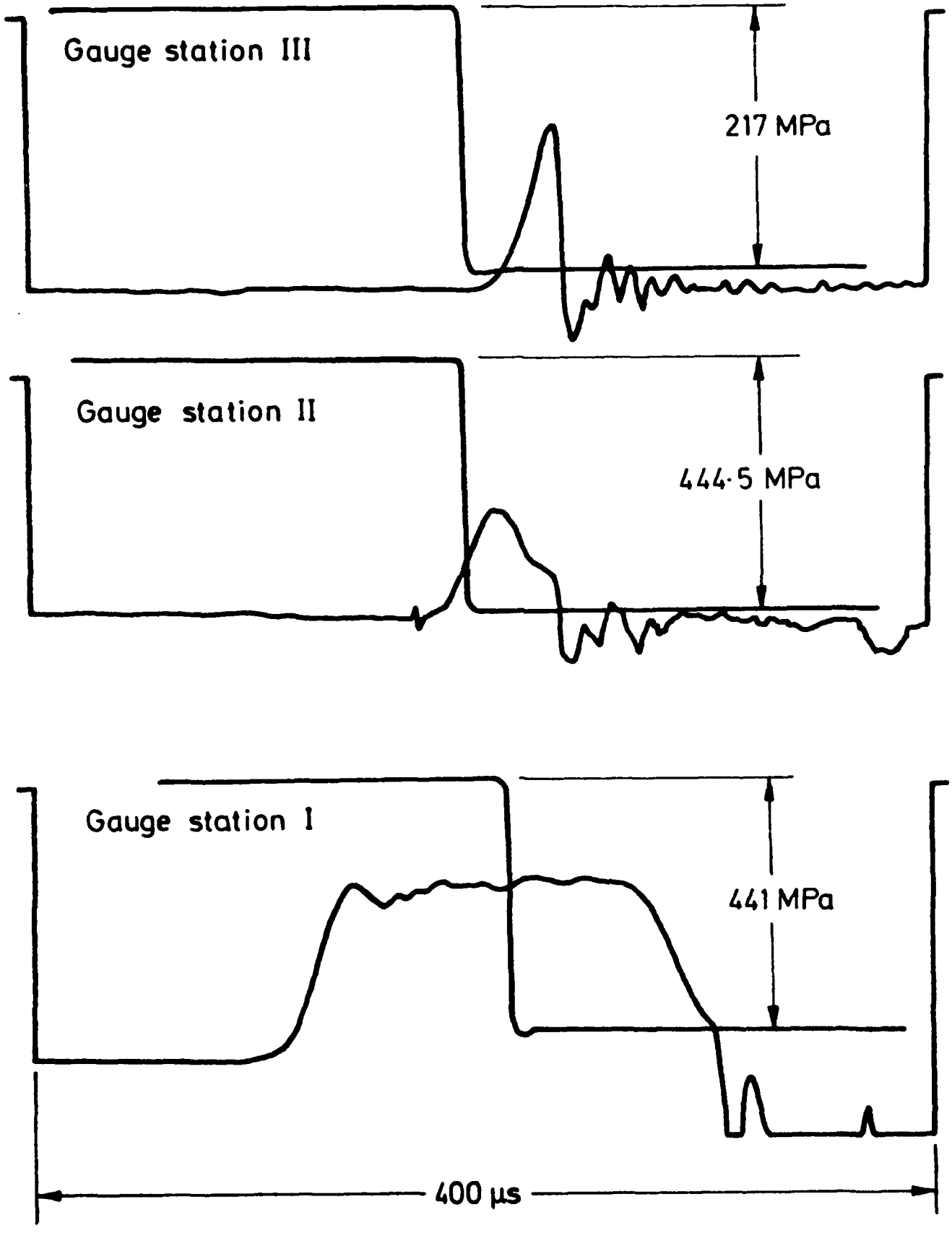

Fig.16 STRAIN-GAUGE SIGNALS FOR IMPACT TEST ON WOVEN CFRP SPECIMEN

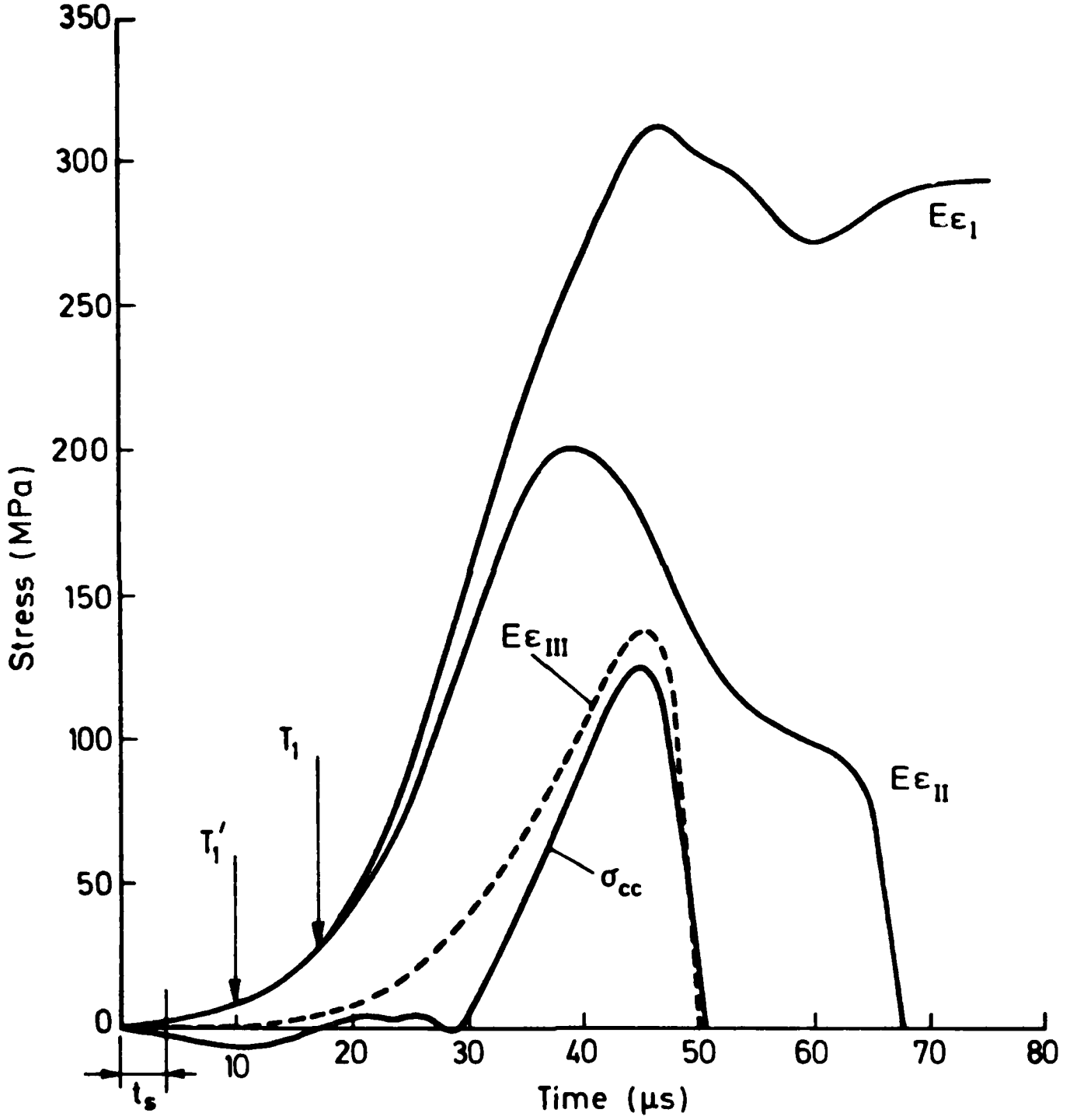

Fig.17 HOPKINSON-BAR ANALYSIS FOR TEST OF Fig.16

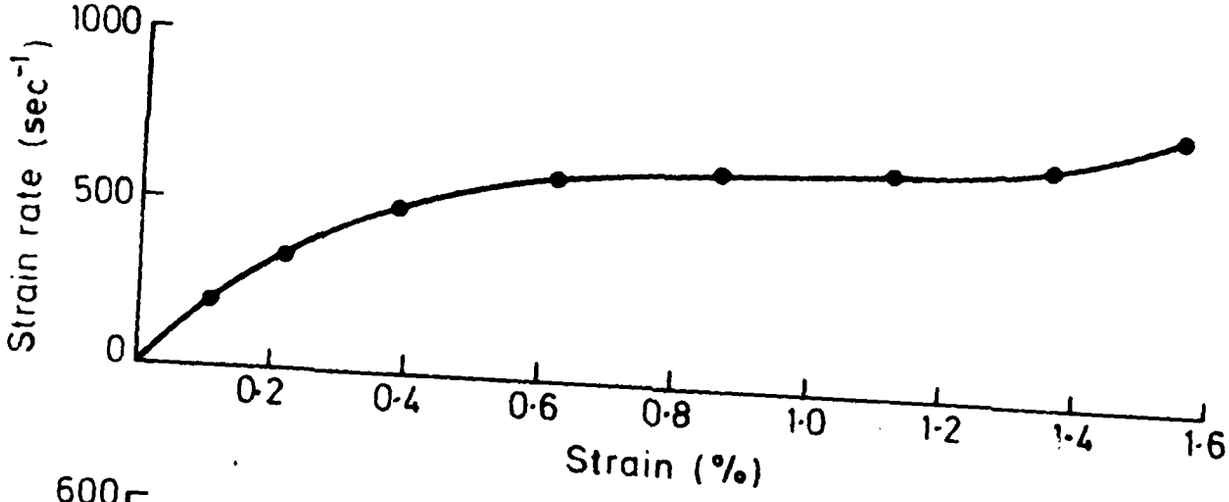

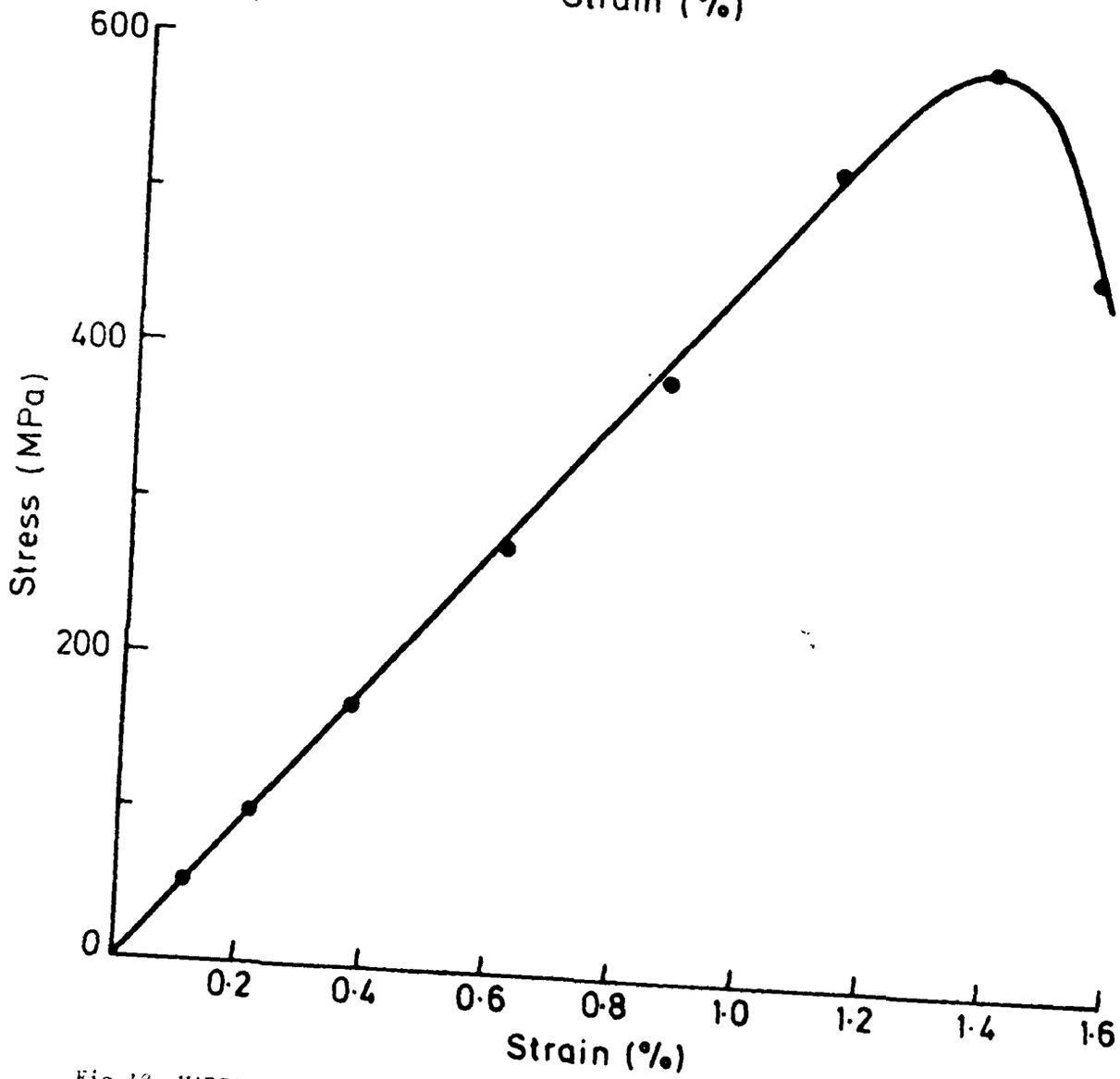

Fig.18 VARIATION OF STRESS WITH STRAIN AND STRAIN RATE WITH STRAIN FOR TEST ON WOVEN CFRP SPECIMEN OF Fig.16

In practice however, comparison of traces I and II shows that a slight reduction in the estimated time delay between them, by 2 μs in about 70 μs, gives a better correlation over the early stages, $t<T_1'$ or $t<T_1$, where they are expected to be identical. The corresponding adjustment in the time zero for trace III leads to the close agreement between the $E\varepsilon_{III}$ and σ_{cc} traces shown in fig. 17, both falling to zero stress at the same time of 50 μs. Before making this adjustment the apparent modulus had been 44.6 GPa, about 4% less than the value quoted above, the strain at fracture was about 1.58% and the initial part of the stress-strain curve, up to a stress of about 200 MPa, was non-linear. This relatively small uncertainty in the specimen modulus and fracture strain is, perhaps, acceptable, especially in view of the expectation that by attaching strain gauges directly to the specimen a further independent check of specimen strain may be made.

The results showed somewhat less satisfactory agreement, however, in the test on the carbon-glass type 1 hybrid. Here, using the same technique for determining the time zero's for the three stress-time traces and then adjusting again by 2 μs gave a discrepancy of 7 μs in the times at which the input and output stress pulses fell to zero. The corresponding stress-strain curve was again initially non-linear to a stress of about 200 MPa followed by a linear region with an apparent modulus of 24.6 GPa. If, however, the $E\varepsilon_{III}$ trace was shifted by this amount, ie., it was assumed that the delay between traces II and III had been over-estimated by 7 μs, then the resulting dynamic stress-strain curve was linear from the start of loading to over 400 MPa and the corresponding modulus was 31.4 GPa. Thus a 7 μs shift in the output trace leads to a 25% increase in the modulus. This is clearly too large a discrepancy to be acceptable and further work with strain gauges on the specimen is required before firm conclusions can be drawn. For the present report, however, the linear stress-strain response corresponding to the input and output traces falling to zero at the same time is assumed to give the best representation of the specimen response and it is these results which are quoted in subsequent discussion.

Collected results for the modulus, fracture strength and fracture strain as a function of the hybrid fraction, defined as the weight of carbon to the total weight of reinforcement in the parallel gauge section, are presented in figs. 19 and 20. Except for all-carbon material the results quoted are derived from a single test on each type of specimen. Further tests will, therefore, be required to confirm the trends observed. For the all-carbon reinforced material five tests have been performed, giving a range in the observed fracture strength, defined as the maximum stress reached just before failure, of 560 MPa to 598 MPa, ie., a scatter of about $\pm$ 7%. In only one of these tests, however, was a reliable measure of modulus and failure strain possible so again further tests will be required. The general response of the all-carbon and the three types of hybrid specimen under impact loading was very similar and is typified by the output ($E\varepsilon_{III}$) stress-time trace for one such test shown in fig. 21a. A rather different behaviour was shown in the test on an all-glass specimen. The output stress-time trace for this specimen is shown in fig. 21b and the corresponding stress-strain curve in fig. 22.

The marked stress fluctuations following the initial elastic line are thought to be genuine and to represent the progressive damage developing in the specimen before final failure at a strain of about 4.5%, as compared with the other types of specimen where failure in each case was at a strain of less than 2%. This difference in response suggests a difference in the mechanisms controlling fracture and prevents a direct comparison between the fracture strength and fracture strain for the two types of specimen. Thus, while for the hybrid and the all-carbon specimens the fracture strength is taken at the peak load on the output stress-time trace and the fracture strain at the corresponding point on the derived stress-strain curve, no similarly clear definition is possible for the all-glass specimen. For the purposes of the comparison in fig. 20, therefore, the fracture strength has been assumed to lie within a range from that corresponding to the limit of the elastic region, ie., where the first signs of damage appear, up to the peak of the largest stress fluctuation while the fracture strain has been taken to correspond to some point on the stress-strain curve between the elastic limit and the final rapid fall off in stress at the end of the test.

Thus, while the modulus for the all-glass specimen lies on the extrapolation of the line through those for the hybrid and all-carbon specimens, see fig. 19, the fracture strength and fracture strain of the all-glass specimen only behave in the same way if fracture is associated with the first signs of damage on the stress-strain curve, see fig. 20. This would seem to imply that the mechanism of failure initiation is the same for all specimens but that, while in the presence of sufficient carbon reinforcement, in this case 0.4 or more by weight, propagation of failure is catastrophically rapid, for the all-glass reinforcement the propagation stage covers the major part of the overall deformation. It should be noted that if the hybrid fraction is expressed in terms of the volume, rather than the weight, of carbon the gap between the all-glass and the hybrid specimens in figs. 19 and 20 is increased to about 0.49. While not invalidating the conclusions drawn from fig. 20 regarding the initiation and propagation of failure this does accentuate the non-linearity of the dependence of modulus on hybrid fraction shown in fig. 19. It also points the need for hybrid specimens with a greater ratio of glass to carbon to fill this gap. To achieve a higher glass content, however, would require a stacking sequence involving three layers of glass mat to each one of carbon, leading to a preponderance of glass/glass interfaces between adjacent reinforcing layers and so introducing another parameter that might possibly affect the mechanical response. In the existing tests only carbon/glass interfaces are present in specimens of types 2a and 2b while for type 1 specimens there are four carbon/glass interfaces to three glass/glass interfaces.

5.2 Model Specimens

As described in section 3.1, model specimens with all glass, all carbon and various carbon/glass hybrid reinforcement configurations were prepared using the same epoxy resin system and reinforcing fibres as previously used in an earlier investigation (5).

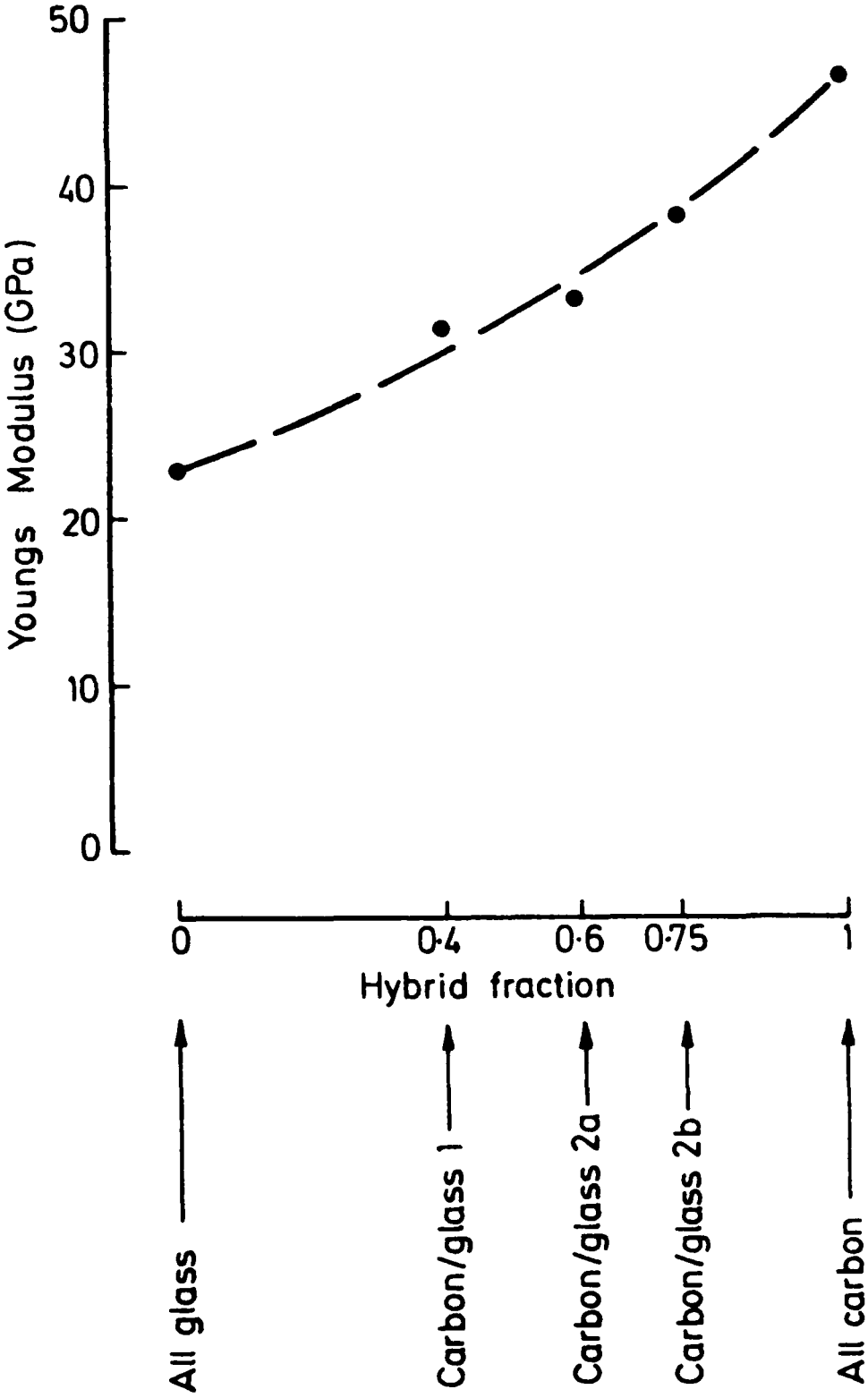

Fig.19 VARIATION OF YOUNGS MODULUS WITH HYBRID FRACTION FOR WOVEN CARBON/GLASS SPECIMENS

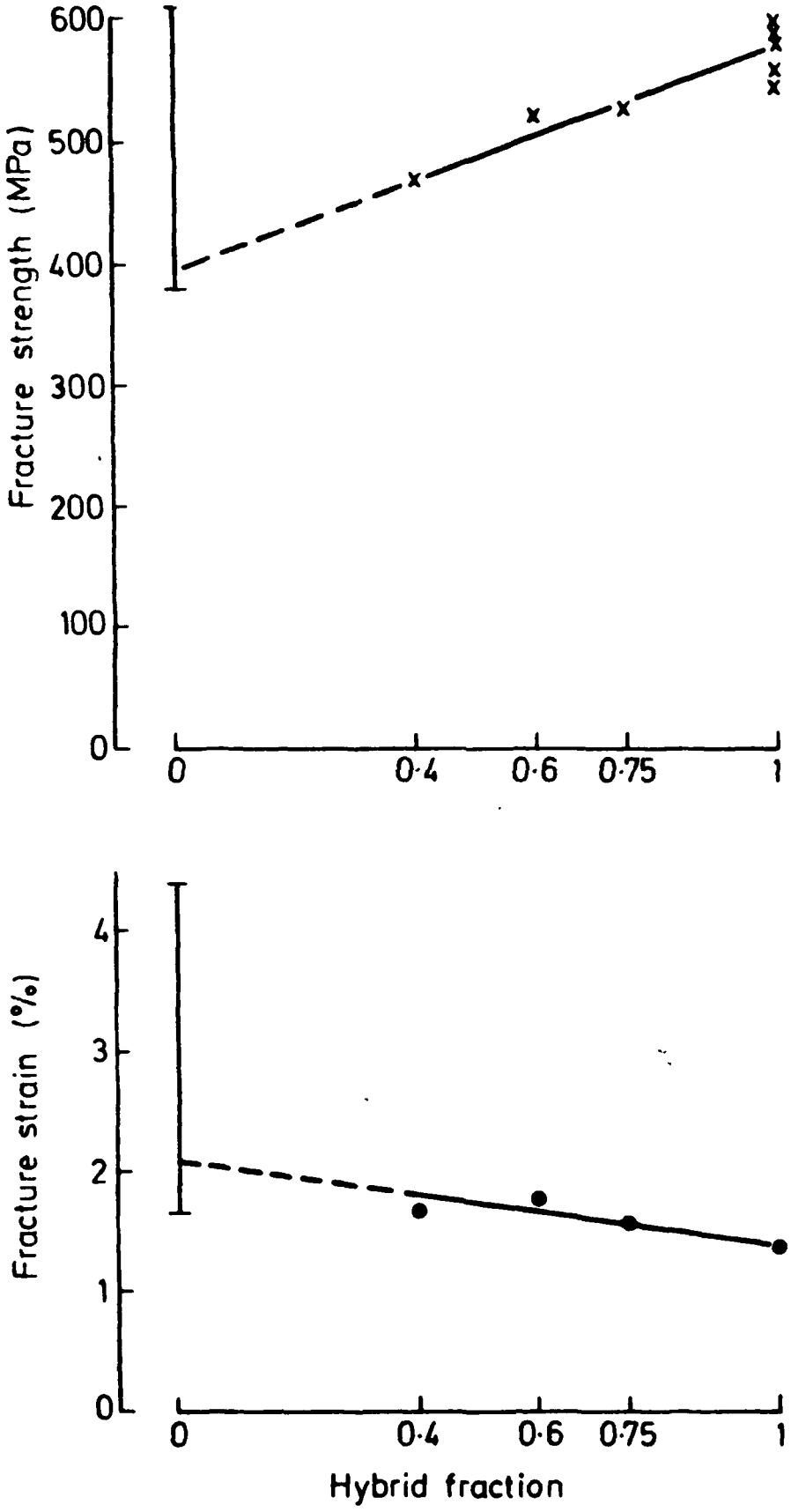

Fig.20 VARIATION OF FRACTURE STRENGTH AND FRACTURE STRAIN WITH HYBRID FRACTION FOR WOVEN CARBON/GLASS SPECIMENS

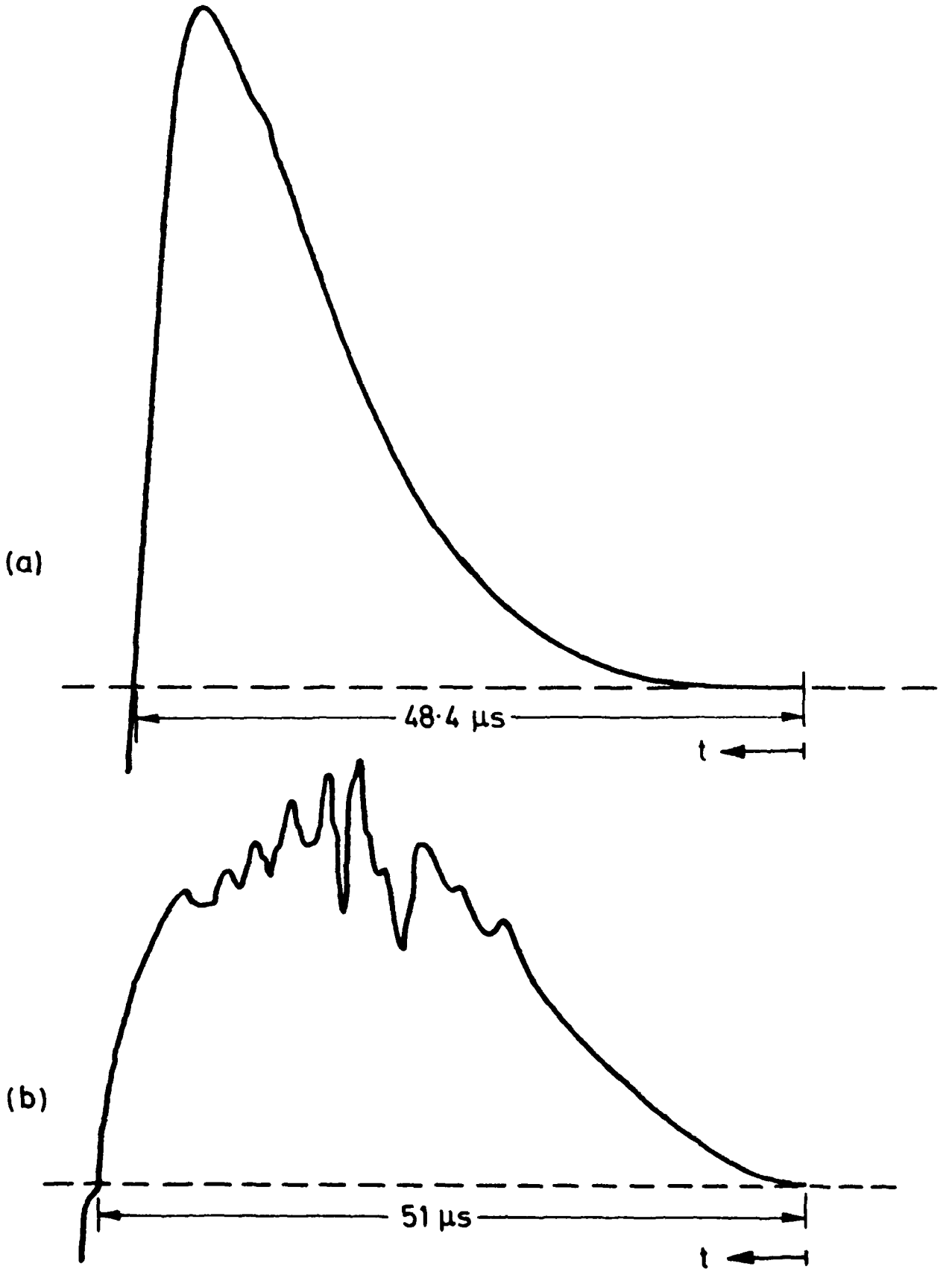

Fig.21 OUTPUT BAR STRAIN-GAUGE SIGNALS

a) Woven CFRP specimen b) Woven GFRP specimen

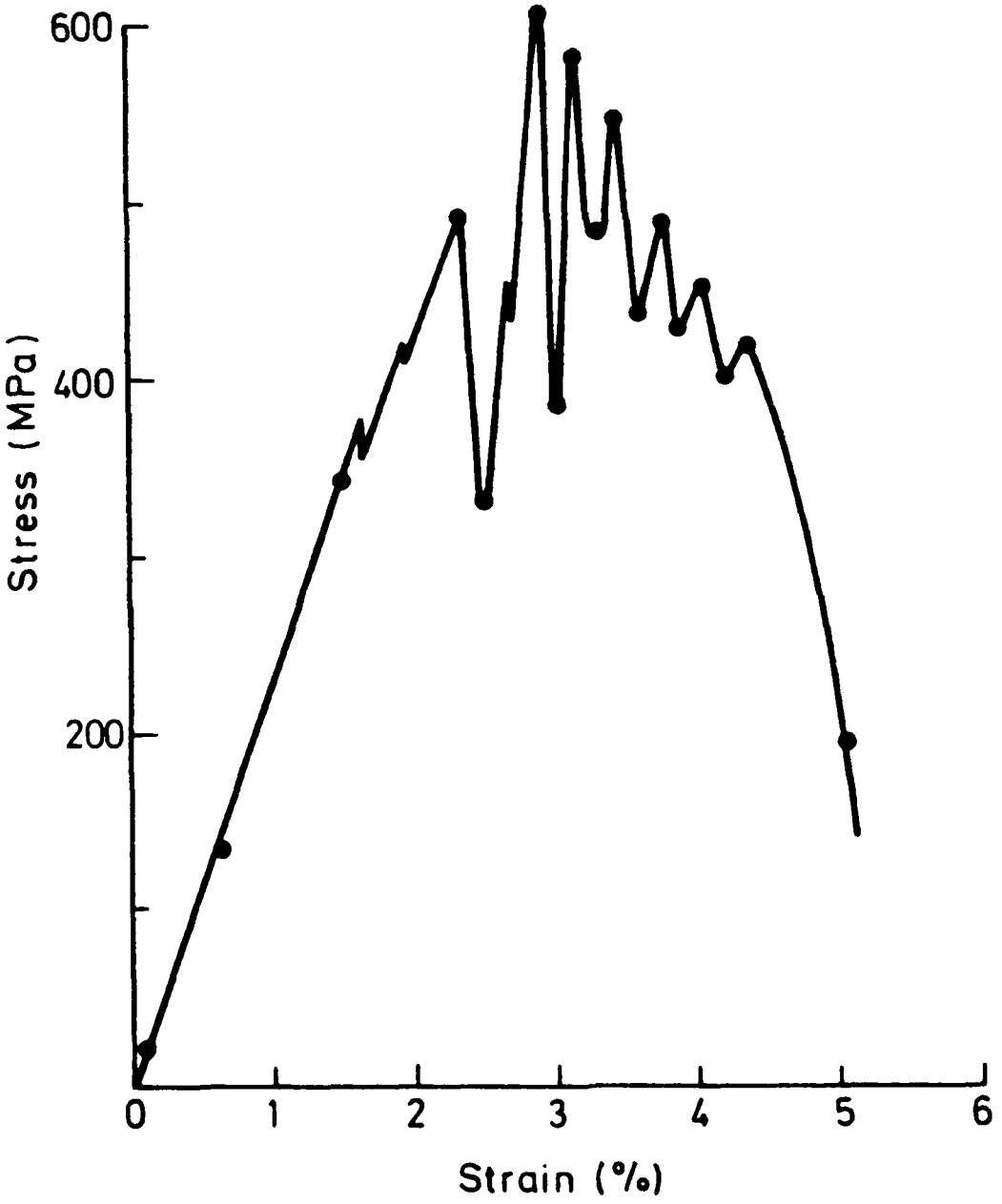

Fig.22 STRESS-STRAIN CURVE FOR IMPACT TEST ON WOVEN GFRP SPECIMEN

The initial aim was to develop the technique for preparing model specimens with a hybrid reinforcement. Subsequently these specimens were used in the early commissioning tests on the extended tensile impact tester. At this stage in the experimental programme several problems became apparent. In particular, these included:

a) electrical interference between the signal from the first set of strain gauges and the subsequent signals from gauge stations II and III, affecting both the lead-in region and superimposing what are thought to be spurious oscillations on the strain gauge signal itself. In such tests it was not possible to analyse the data sufficiently accurately for a dynamic stress-strain curve to be obtained. This problem was eventually eliminated by rewiring the gauges and re-routing the gauge leads.

b) in some, but not all, tests tensile failures occurred, not in the central parallel region of the specimen (as in fig. 15), but at section CC or DD, ie., at the interface between the specimen and one of the loading bars. In one test fracture was thought to have occurred at both specimen/loading-bar interfaces but because of (c) below it was not possible to be certain that the second fracture had not occurred at a later stage. The problem of tensile failure at the specimen ends, with the implication that it was premature failure due to local stress concentrations, seems to arise most frequently in unidirectionally-reinforced specimens. A solution had not been found when the woven-reinforced laminates supplied by Fothergill and Harvey became available and the emphasis of the testing programme changed.

c) following fracture of the specimen, the output bar becomes free of restraint and may rebound from the top end of the hole in the weighbar tube, see fig. 4, so that the two broken halves of the specimen suffer a subsequent compression impact, damaging the original tensile fracture surface. This problem has now been solved by the development of an energy absorbing device which catches the output bar, preventing it from rebounding.

Because of these problems little information on the specimen mechanical response was obtained from this first set of tests on model specimens. In one test, however, on a specimen impacted at 11.8m/s, a peak specimen stress of 291 MPa was obtained. This compares with a peak stress of 190 MPa in a quasi-static test on a similar specimen. A marked effect or strain rate on the fracture strength is indicated, such as, in the absence of any quasi-static tests, has not yet been demonstrated in the woven-reinforced specimens.

5.3 Examination of Failure Modes

Macrographs of the fracture regions of the two model specimens referred to in section 5.2 are shown in figs. 23a and 23b, for the impact and the quasi-static tests respectively. Both specimens were reinforced with three carbon fibre tows and two glass fibre tows.

In the quasi-static test the fracture appearance suggests the possibility that a flaw in one of the glass fibre tows may have led to premature fracture at a stress below that which might have been expected in an unflawed specimen, implying that the true rate dependence of the fracture strength is, perhaps, not as great as these results might lead us to believe. In the impact test, also, much greater damage is apparent in the glass than in the carbon reinforced regions. Here, however, the damage is more equally divided between the two glass reinforced regions.

Macrographs of impacted woven-reinforced specimens are shown in fig. 24a, for the all-glass composite, fig. 24b for the type 1 hybrid composite and fig. 24c for the all-carbon composite. The comparison is partially obscured by the much coarser tow size and weave geometry in the carbon, in contrast to the glass, reinforcing mats. Nevertheless, the all-carbon specimen shows a flatter fracture surface, with damage limited to regions no greater than the wavelength of the weave whereas the all-glass specimen shows a much less flat fracture surface with damage and fibre pull-out extending, relative to the wavelength of the weave, over a zone an order of magnitude greater and with separation between the orthogonally-aligned rovings in the fracture region playing a much greater part in the overall failure process.

The type 1 hybrid, which has a carbon to glass weight fraction of 0.4, the lowest of the three hybrids tested, showed an intermediate response, see fig. 24b, with some separation of the orthogonally-aligned rovings in the glass mats and damage extending over several wavelengths of the glass weave. A similar behaviour was also shown in fig. 15, for the type 2a hybrid with a carbon to glass weight fraction of 0.6. It is apparent that the clear distinction in mechanical response between the all-carbon and the three hybrid composites, on the one hand, and the all-glass composite, on the other, see figs. 20 and 21, is not reflected in the fracture appearance where the clearest distinction is between the all-carbon composite on the one hand and the all-glass and the three hybrid composites on the other. Thus, while a carbon weight fraction of 0.4 or more leads to a near linear-elastic stress-strain response, the fine weave glass reinforcement dominates the fracture appearance for carbon weight fractions up to at least 0.6.

In an attempt to describe the fracture process in more detail the three specimens shown in fig. 24 have also been examined in a scanning electron microscope. The fracture surfaces observed at a magnification of x28 are compared in figs. 25a, b and c for the all-glass, the type 1 hybrid and the all-carbon specimens respectively. Although the quality of the scanning electron micrographs obtained leaves much to be desired, they do confirm the observations made from the optical macrographs. Further work on the examination of failure modes using the scanning electron microscope will continue.

a) Impact test (x11)

b) Quasi-static test (x4.3)

Fig.23 FAILURE MODES FOR TESTS ON MODEL SPECIMENS

a) All-glass reinforcement

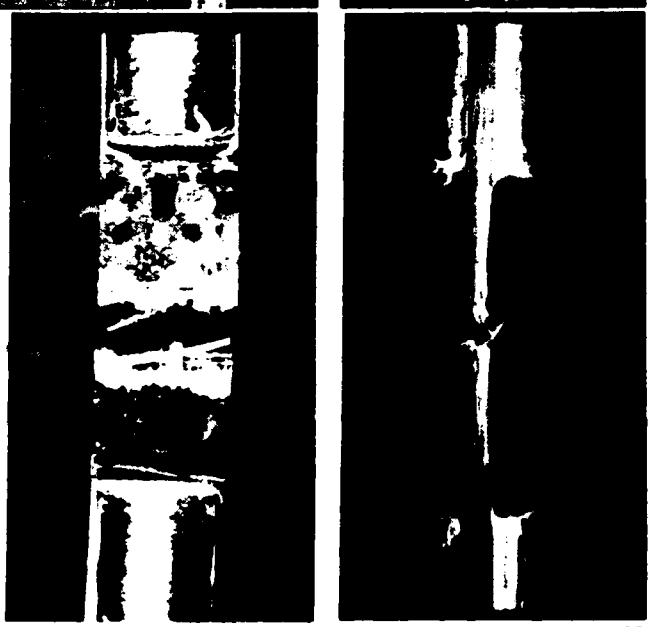

b) Type I carbon/glass hybrid

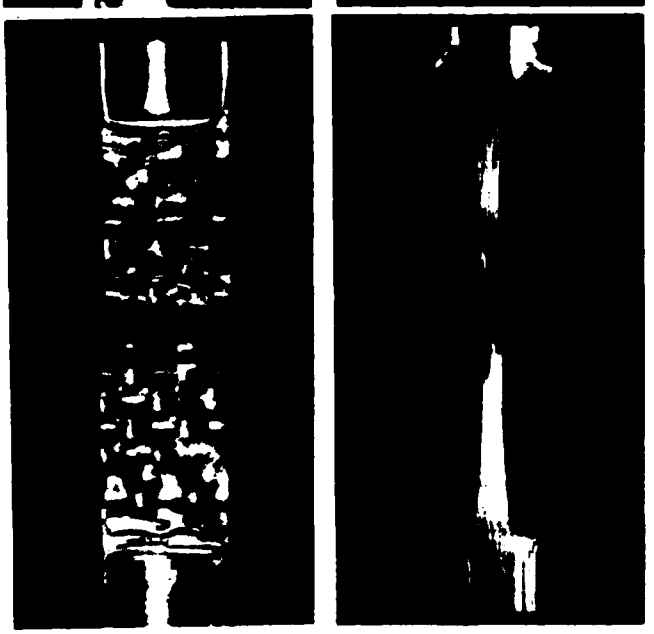

c) All-carbon reinforcement

Fig.24 FAILURE MODES FOR WOVEN CARBON/GLASS SPECIMENS

a) All-glass reinforcement

b) Type 1 carbon/glass hybrid

c) All-carbon reinforcement

Fig.25 SCANNING ELECTRON MICROGRAPHS OF THE FRACTURE SURFACES OF THE SPECIMENS OF Fig. 24 (x28)

6. CONCLUSIONS

1. A gas gun has been built capable of accelerating a projectile, 1 m long by 25.4 mm diameter, to a velocity of about 50 m/s.

2. An extended version of the tensile SHPB has been developed in which fibre-reinforced composite specimens may be tested at rates of the order of 1000/s and a full wave analysis performed in both input and output loading bars for test durations up to 150 μs.

3. Even in the most extreme case, ie., for a relatively thick specimen of a low-modulus glass-reinforced composite, allowance for the effect of stress-wave reflections in the grip regions is found to modify only very slightly the calculated dynamic stress-strain curve.

4. Reasonably good agreement between the stress levels determined at the specimen input and output interfaces is obtained, confirming that a uniform stress state in the specimen may be assumed from an early stage in the test. However, some anomalies arising from the analysis still require further study and additional calibration tests using an extra set of strain gauges attached directly to the specimen are recommended.

5. Model hybrid specimens of low volume fraction, unidirectionally reinforced with a single layer of fibre tows, alternately of carbon and of glass, have been successfully prepared. In impact tests on these specimens a tendency to fail at the interface with one of the loading bars, rather than in the central parallel gauge section, has not yet been successfully overcome.

6. Commercially supplied high volume fraction woven reinforced laminates have been obtained, in which carbon, glass and kevlar plain weave reinforcing mats are arranged in a variety of lay-ups so as to allow the preparation of hybrid specimens with three different carbon to glass and three different carbon to kevlar weight fractions.

7. An initial set of impact tests has been performed on woven specimens with an all-glass, an all-carbon and each of the three carbon/glass hybrid reinforcement configurations. The three hybrid materials and the all-carbon composite show a similar mechanical behaviour, with a linear-elastic stress-strain response to within about 10% of the maximum load, followed by a small region of anelastic deformation with failure following immediately after the attainment of maximum load. The modulus and the maximum (or fracture) stress increase continuously and the fracture strain decreases continuously the higher the proportion of carbon fibres in the hybrid fraction. Although the modulus of the all-glass specimen behaves in a similar way the dynamic stress-strain curve for this material shows a much more extended region of anelastic deformation and comparable values for fracture strength and fracture strain cannot be determined.

8. Optical examination of model specimens shows that at both quasi-static and impact rates the glass regions of carbon/glass hybrids sustain the bulk of the damage. Similar observations, both by optical examination and by scanning electron microscopy, for the woven-reinforced composites, although partially obscured by the large difference in weave count between the carbon and the glass reinforcing mats, lead again to the same conclusion.

7. FUTURE WORK

The work described in this report is being continued on a new Research Grant, No. AFOSR-84-0092. It is anticipated that the first steps to be taken in this next stage of the work will include the following:

1. A further validation of the impact testing procedure by the use of an additional set of strain gauges attached directly to the specimen.

2. A confirmation of the trends in mechanical response shown in the initial set of impact tests on carbon/glass hybrids by increasing the number of tests on each type of specimen.

3. An extension of the test programme to include results at lower strain rates and on specimens having a carbon/kevlar hybrid reinforcement.

4. Preparation of models specimens using the epoxy resin system and the same fibre reinforcement tows as in the commercially supplied woven-reinforced laminates.

5. An attempt to minimise failures in model specimens at the specimen/loading bar interfaces by suitable modifications to the specimen design or the loading bar dimensions in the grip regions.

6. More detailed studies of the damage associated with failure in the various types of specimen at different loading rates by optical and scanning electron microscopy.

In the longer term, it is planned also to:

7. Modify the gas-gun loading system to allow the tensile impact testing of composites at temperatures other than ambient and,

8. Investigate modified specimen gripping techniques so as to obtain tensile failures in unidirectionally reinforced GFRP and glass/carbon hybrid specimens of higher volume fraction.

* * * * * * * *

8. APPENDIX

The loading-bar/specimen/output-bar assembly is shown in fig. A1, divided into five regions of different effective acoustic impedance. If the change in impedance between regions 1 and 2 and between regions 4 and 5 is sufficiently great, stress waves may be reflected at these interfaces, giving the wave propagation pattern shown schematically in the figure. Both the input and the output bars have a diameter of 3/8 in (9.525mm) and both are centreless ground, the former from an annealed IMI318 titanium alloy and the latter from an annealed phosphor bronze alloy. The corresponding values of density, ρ, Youngs modulus, E, longitudinal elastic wave speed, c, acoustic impedance, ρc, and driving point impedance, ρcA (where A is the cross-sectional area), are listed in Table 1 below. Also included in the Table are similar data for a woven-glass reinforced epoxy composite specimen loaded in the 45^{o} orientation taken from earlier work (2). In the grip regions, i.e. regions 2 and 4, effective values of density and modulus are derived using the rule of mixtures and the relative areas of cross-section of the bar and the specimen. The effective wave speed is then taken as $\sqrt{E/\rho}$ in the normal way.

Table 1 Estimated Impedances for Loading-Bar/Specimen Assembly

Region		1	2	3	4	5
ρ	(kg/m^3)	4431	3260	1885	5676	8906
c	(m/s)	5106	4660	3116	3554	3627
E	(GPa)	115.5	70.8	18.3	71.7	117.2
ρc	($kg/m^2\mu s$)	22.62	15.19	5.87	20.17	32.30
ρcA	(kg/s)	1612	1083	192.5	1437	2302

To analyse for the effect of reflected waves in the grip region of the input bar the method of characteristics is used, as illustrated in fig. A2. Referring to this figure, for all points between A and C, corresponding to the position of gauge station II, the input wave at times $< T_1'$ is given by

$$\alpha_1 = E\varepsilon_I = E\varepsilon_{II} \qquad (A1)$$

while for all points along $ACC_1C_2....$, to the limiting time T_2', the relation

$$\alpha_1 = E\varepsilon_I \qquad (A2)$$

still holds.

At the interface between the loading-bar and the grip region, i.e. for points along $BDD_1...$ in fig. A2, for times $< T_3'$ elementary one-dimensional longitudinal elastic wave theory gives the relations

$$\alpha_2 = \{2Z_2/(Z_2 + Z_1)\}(A_1/A_2)\alpha_1 \qquad (A3)$$

$$\beta_1 = \{(Z_2 - Z_1)/(Z_2 + Z_1)\}\alpha_1 \qquad (A4)$$

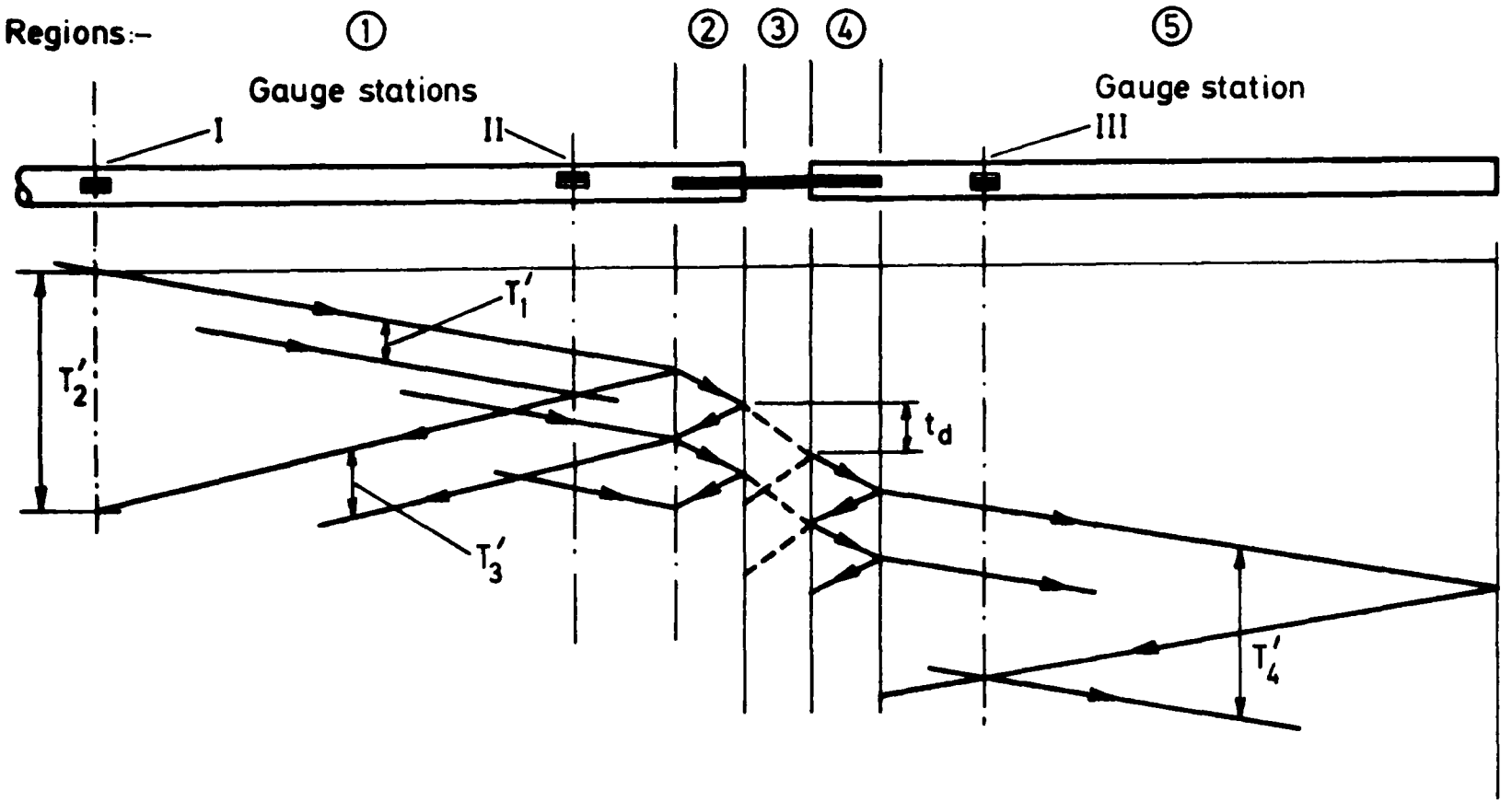

Fig.A1 LOADING-BAR/SPECIMEN ASSEMBLY AND LAGRANGE DIAGRAM FOR WAVE REFLECTIONS IN SPECIMEN GRIP REGIONS

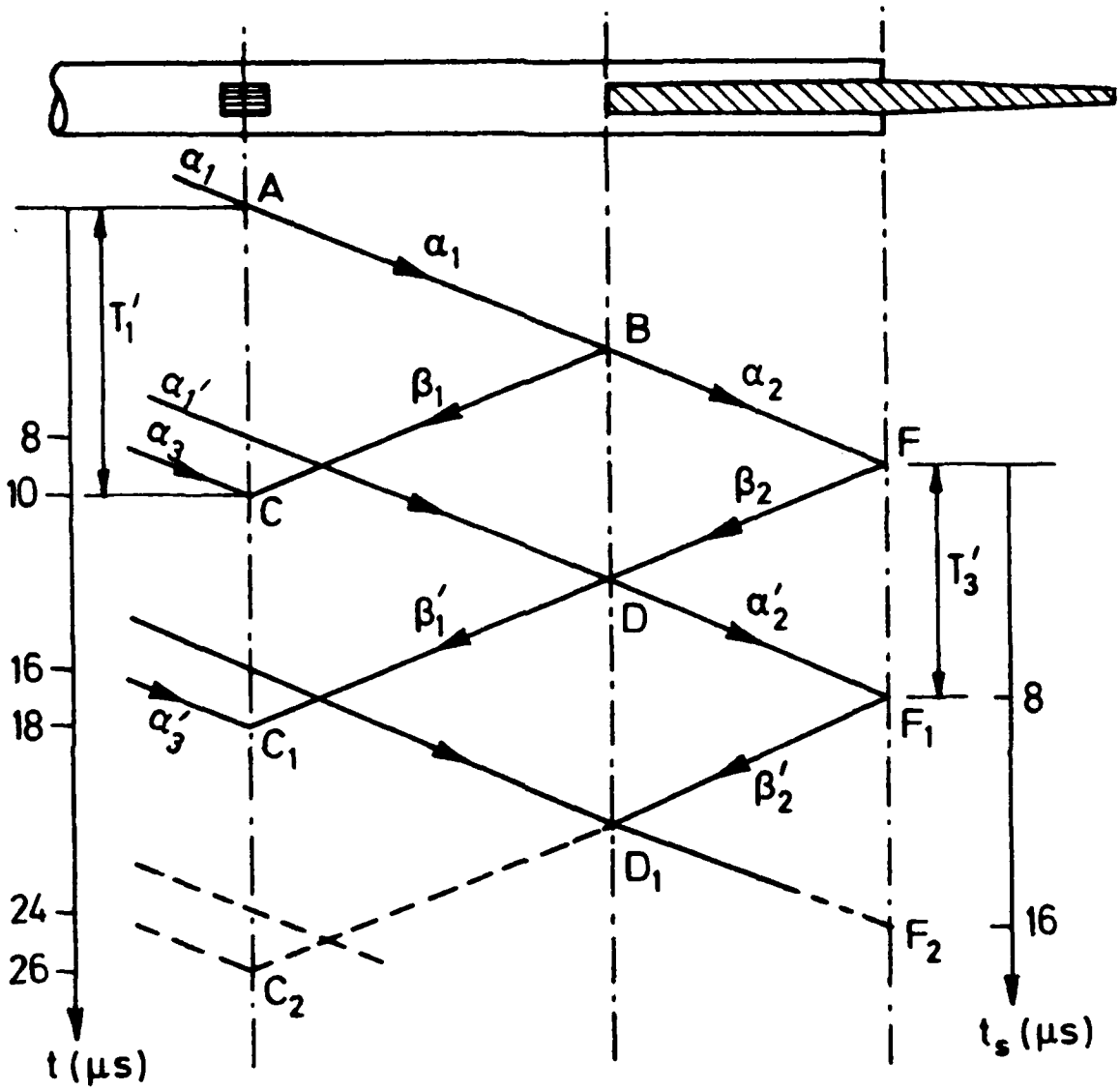

Fig.A2 WAVE ANALYSIS FOR GRIP REGION OF INPUT BAR

where $Z = \rho cA$ is the effective driving point impedance in the given region. Since α_1, Z_1 and Z_2 are known, α_2 and β_1 may be calculated.

The reflected β wave from the interface represented by $BDD_1...$ interacts with the incident α wave at gauge station II represented by $CC_1C_2...$ such that at a point such as C_1, for example, for which the time is given by $T_1' < t < T_2'$, the relations

$$\alpha_3' = E\varepsilon_I \tag{A5}$$

$$\beta_1' + \alpha_3' = E\varepsilon_{II} \tag{A6}$$

hold, allowing the determination of β_1'. At the interface $BDD_1...$ for points from D onwards, i.e. for times given by $T_3' < t < T_2'$, the relations (A3) and (A4) are modified to become

$$\alpha_2' = \{(Z_1 - Z_2)/(Z_1 + Z_2)\}\beta_2 + \{2Z_2/(Z_1 + Z_2)\}(A_1/A_2)\alpha_1' \tag{A7}$$

$$\beta_1' = \{(Z_2 - Z_1)/(Z_2 + Z_1)\}\alpha_1' + \{2Z_1/(Z_1 + Z_2)\}(A_2/A_1)\beta_2 \tag{A8}$$

Since β_1' has been obtained from (A5) and (A6) and α_1' is given by (A2) at the appropriate time, t, equations (A7) and (A8) may be solved to give β_2 and α_2'. Finally the stress and particle velocity at, for example, point F on the loading-bar/specimen interface may be obtained from the relations

$$\sigma = \beta_2 + \alpha_2 \tag{A9}$$

and $$v = (\beta_2 - \alpha_2)/\{(\rho c)_2\} \tag{A10}$$

where $(\rho c)_2$ is the acoustic impedance in region 2, the grip region of the input bar. The calculation proceeds in a stepwise manner up to the limit at $t = T_2'$.

The analysis of wave reflections in the grip region of the output bar, see fig. A3, is rather simpler. For times, $t < T_4'$, where T_4' is defined in fig. A1, we have

$$\alpha_5 = E\varepsilon_{III} \tag{A11}$$

while for points along $GG_1...$ the relations

$$\alpha_4 = \{(Z_5 + Z_4)/2Z_5\}(A_5/A_4)\alpha_5 \tag{A12}$$

$$\beta_4 = \{(Z_5 - Z_4)/2Z_5\}(A_5/A_4)\alpha_5 \tag{A13}$$

hold. Thus β_4, determined at point G, and α_4', determined at point G_1, may be combined to give the stress and particle velocity at point H, on the specimen/output-bar interface, using the relations

$$\sigma = \beta_4 + \alpha_4' \tag{A14}$$

and $$v = (\beta_4 - \alpha_4')/\{(\rho c)_4\} \tag{A15}$$

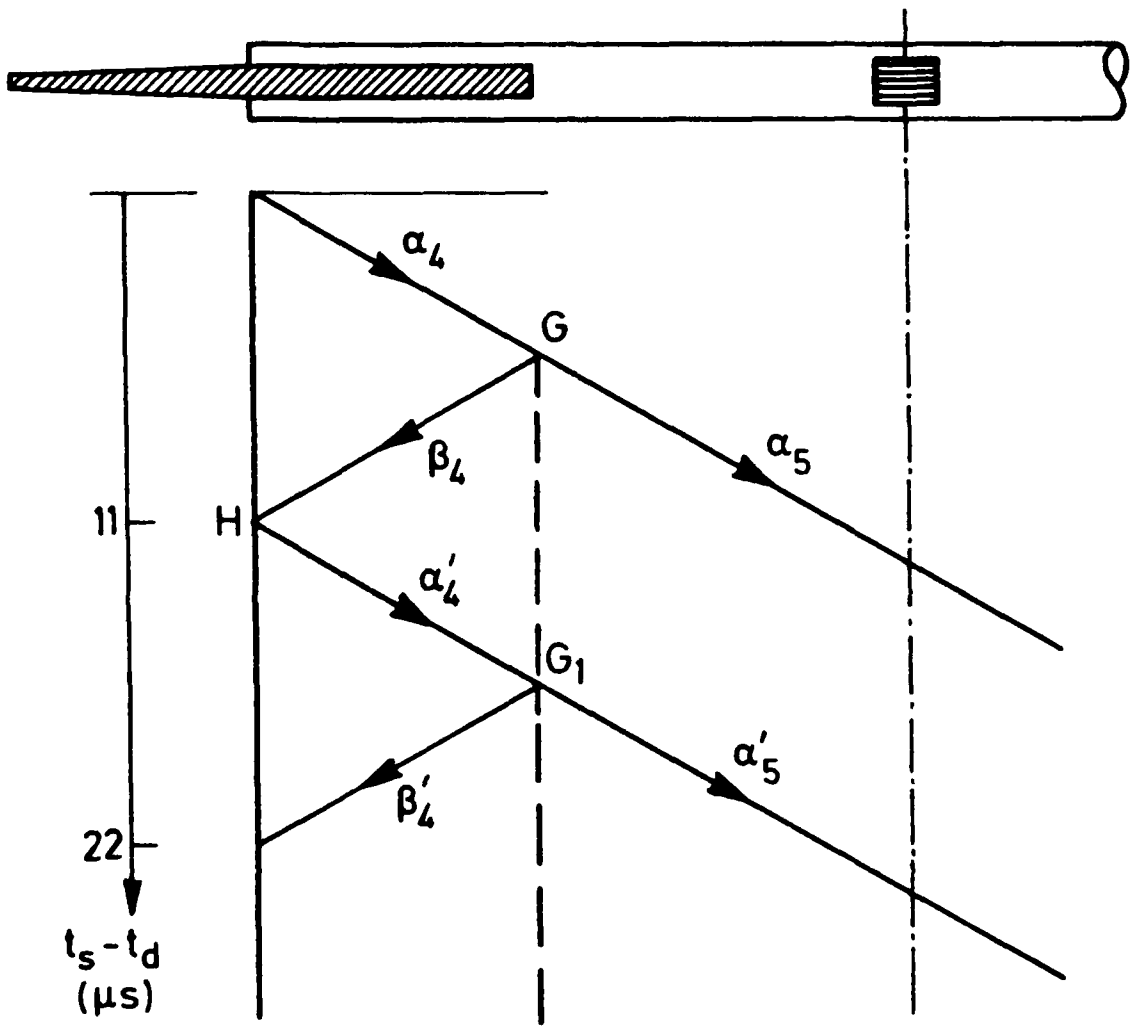

Fig.A3 WAVE ANALYSIS FOR GRIP REGION OF OUTPUT BAR

END

FILMED

3-85

DTIC